Dissipative Homogenised Reinforced Concrete (DHRC) constitutive model dedicated to reinforced concrete plates under seismic loading

Christelle Combescure, Hélène Dumontet, François Voldoire

▶ **To cite this version:**

Christelle Combescure, Hélène Dumontet, François Voldoire. Dissipative Homogenised Reinforced Concrete (DHRC) constitutive model dedicated to reinforced concrete plates under seismic loading. International Journal of Solids and Structures, 2015, 73-74, pp.78 - 98. 10.1016/j.ijsolstr.2015.07.007 . hal-01654799

HAL Id: hal-01654799

https://inria.hal.science/hal-01654799

Submitted on 4 Dec 2017

HAL is a multi-disciplinary open access archive for the deposit and dissemination of scientific research documents, whether they are published or not. The documents may come from teaching and research institutions in France or abroad, or from public or private research centers.

L'archive ouverte pluridisciplinaire **HAL**, est destinée au dépôt et à la diffusion de documents scientifiques de niveau recherche, publiés ou non, émanant des établissements d'enseignement et de recherche français ou étrangers, des laboratoires publics ou privés.

International Journal of Solids and Structures 73–74 (2015) 78–98

Contents lists available at ScienceDirect

International Journal of Solids and Structures

journal homepage: www.elsevier.com/locate/ijsolstr

Dissipative Homogenised Reinforced Concrete (DHRC) constitutive model dedicated to reinforced concrete plates under seismic loading

Christelle Combescure [a,b,c,*], Hélène Dumontet [c], François Voldoire [a,b]

[a] Électricité de France, R&D/AMA, 1, Avenue du Général de Gaulle, F-92141 Clamart, France
[b] Institute of Mechanical Sciences and Industrial Applications, EDF–CNRS–CEA–ENSTA UMR 9219, 1, Avenue du Général de Gaulle, F-92141 Clamart, France
[c] Univ. Paris VI, UMR CNRS 7190, Institut Jean Le Rond d'Alembert, 4, place Jussieu, F-75252 Paris Cedex 05, France

ARTICLE INFO

Article history:
Received 24 February 2015
Received in revised form 8 May 2015
Available online 16 July 2015

Keywords:
Constitutive model
Reinforced concrete
Debonding
Damage
Plate
Periodic non linear homogenisation
Seismic loading

ABSTRACT

A new stress resultant nonlinear dissipative constitutive model for reinforced concrete (RC) plates under cyclic solicitations is presented. This constitutive model, named DHRC for Dissipative Homogenised Reinforced Concrete, is expressed within the usual thin plate kinematics framework. It is built by a periodic homogenisation approach using the averaging method and it couples concrete damage and periodic debonding between steel rebar and surrounding concrete. The generality of the proposed method leads to a generic closed-form for the Helmholtz strain energy density function and the two dissipation pseudo-potentials that can be adapted to any material with an internal structure similar to the RC structural element one. A restricted number of geometric and material characteristics are needed from which the whole set of model parameters are identified through an automatic numeric procedure performed on a Representative Volume Elements (RVEs) of the RC plate. Finally, comparisons of finite element simulations with experimental results concerning the seismic behaviour of reinforced concrete wall made structures are proposed and discussed.

© 2015 Elsevier Ltd. All rights reserved.

1. Introduction

1.1. Context

Many industrial facilities, in particular power generation plants, are composed with large and complex reinforced concrete (RC) buildings. Severe structural strength requirements (for instance under several external aggression such as seismic loading or severe wind) have often to be considered. Both conceptual design and periodic re-examination during life-duration require practitioners to perform best-estimate numerical analyses, accounting for the nonlinear behaviour of materials. However, only a few numbers of realistic nonlinear constitutive models dedicated to RC slabs and walls exist, ensuring rational computational costs, numerical efficiency and robustness for whole finite element analysis, in particular for cyclic and dynamic loadings. Stress resultant plate and shell models are frequently used in civil engineering due to their efficiency in modelling strategy. As far as the nonlinear cyclic behaviour of RC structural elements is considered, we are interested in the nonlinear stiffness reduction and the dissipated energy modelling, both items being key-factors in the dynamic response. They require a proper micromechanical approach, to justify the constitutive parameters chosen to describe the structural response.

The present paper is a direct continuation of the previous work by Combescure et al. (2013), where one could find a detailed overview of the state of the art, and in particular, the overall framework used to formulate a homogenised resultant nonlinear constitutive model for RC members, based on the averaging method applied to plates, see for instance (Caillerie and Nedelec, 1984; Ciarlet, 1979) and the main assumptions done to formulate the overall potentials of the constitutive model, based on the Generalised Standard Materials theory (Halphen and Nguyen, 1975; Sanchez-Palencia et al., 1987; Suquet, 1993). That first paper proposed a one dimensional closed-form model for RC members under cyclic solicitations, used to assess the ability of the homogenisation theoretical framework and the chosen assumptions to produce a nonlinear constitutive model addressing in a suitable manner the initial engineering needs. Then, we presented a one-dimensional stress resultant nonlinear constitutive model for members under cyclic solicitations. That formulation is hereafter extended to the so-called DHRC (Dissipative Homogenised Reinforced Concrete) stress resultant RC plate model, which includes membrane-bending coupling, needed by general modelling situations.

* Corresponding author at: Électricité de France, R&D/AMA, 1, Avenue du Général de Gaulle, F-92141 Clamart, France.
E-mail addresses: christelle.combescure@gmail.com (C. Combescure), helene.dumontet@upmc.fr (H. Dumontet), francois.voldoire@edf.fr (F. Voldoire).

http://dx.doi.org/10.1016/j.ijsolstr.2015.07.007
0020-7683/© 2015 Elsevier Ltd. All rights reserved.

1.2. Selected phenomena to model overview

The following section gathers the selected phenomena to model.

We assume an isothermal linear elastic, isotropic initial state of each material in the RVE. The assumptions related to local microscopic constitutive relations are gathered hereafter. First, steel reinforcement is assumed to be linear elastic.

In the following, we do not represent strain rate effect on the RC properties (e.g. concrete and steel strengths) even if this effect becomes relevant from strain rates about 10^{-2} s^{-1} (Asprone et al., 2012). Indeed, neglecting this effect can be seen as conservative and this study focuses on stiffness reduction and dissipative processes affecting the structural behaviour or RC elements and available safety margins in order to reproduce the experimentally observed highly pinched hysteresis load–displacement curves for low span RC shear walls under seismic loading, or for alternate axial loading on RC members (cf Fig. 1-1).

Microscopic crack distribution in concrete is modelled by means of damage mechanics, without defining a separate damage variable for concrete in tension and compression, according to the Continuum damage mechanics (Kachanov, 1958). For the sake of simplicity, we assume a scalar measure of damage since we can nevertheless represent anisotropic effects on stiffness by means of appropriate Helmholtz free energy and dissipation potential. As described by Feenstra and De Borst (1996), micro and macro-cracking phenomena in the concrete phase are considered separately: first the onset and development of a homogeneous diffuse micro-cracking resulting in concrete stiffness reduction (or damage), second the apparition of macro-cracks leading to displacement discontinuities on specific surfaces, ensuring a partial stress transfer (aggregate interlock, bridging and expanding effects), (Li et al., 1989). We decided not to account for the latter explicitly, but will represent it by an inhomogeneous distribution of damage within the RVE.

We do not represent the plastic strain in concrete, contrary to more sophisticated models, for instance (Krätzig and Pölling, 2004), considering, for now, that this phenomenon is of minor importance for the desired applications. Similarly, shear force transfer across concrete macro-cracks by aggregate interlock and so-called "bridging effect" is neglected. Indeed, according to Feenstra and De Borst (1996), the effect of aggregate interlock decreases with increasing crack width. Moreover, we neglect the dowel action effect (in shear mode), see Pimentel et al. (2010). The failure of the concrete domain within the RVE arises when diagonal cracks separating diagonal tensile zones (orthogonal to concrete ties – or struts – in compression) have opened enough to cancel the aggregate interlock.

In order to involve both independent processes that are irreversible strains stemming from bond-slip mechanism and concrete damage, we decided to use two dissipation potential functions. This process is inspired from the work of Einav et al. (2007) for plastic strain and damage coupling constitutive models with decoupled dissipation using two "yield surfaces". This may be justified from the experimental observation that damage can happen without equivalent plastic strain associated to bond-slip mechanism.

Bond-slip mechanism is recognised as a major effect controlling the response of reinforced concrete structures under cyclic loading, including damage evolution of concrete, for both plain or ribbed bars (Fernandes et al., 2013; Melo et al., 2011; Murcia-Delso et al., 2011). This mechanism is responsible for the "tension stiffening effect", i.e. the stress transfer from steel rebar to concrete domain located between two cracks, resulting in a contribution of cracked concrete to the RC panel overall stiffness. Bond-slip mechanism can be idealised as a specific interface mechanism at steel–concrete boundary, though it involves localised micro cracking and crushing of concrete. Moreover, this mechanism is able to produce irreversible strains and displacements in the RC panel, associated to larger hysteretic energy dissipation than the contribution from the concrete damage alone. In practice a simple stepped rigid-perfectly plastic bond stress-slip relationship for ordinary plain or ribbed rebar seems to be sufficient to catch the main features of this mechanism (Marti et al., 1998; Pimentel et al., 2010). Indeed, according to the analysis for instance quoted by Anyfantis (2014), for the range of usual steel–concrete relationship modulus $E_{sc} \approx 50000$ MPa/m, usual cohesive strength $\tau_b \approx 10$ MPa, and usual Griffith's fracture toughness $G_{fb} \approx 100$ kJ/m (Eligehausen et al., 1983), we are funded to assume a ductile failure rather than a brittle one for debonding, because the cohesive length scale – which is a parameter aiming at distinguishing the contribution of physical phenomena between fracture mechanics and strength criterion (Bazant and Oh, 1983) – here defined by $l_c = E_{sc}\frac{G_{fb}}{\tau_b^2} \approx 50$ m is much larger than the RC

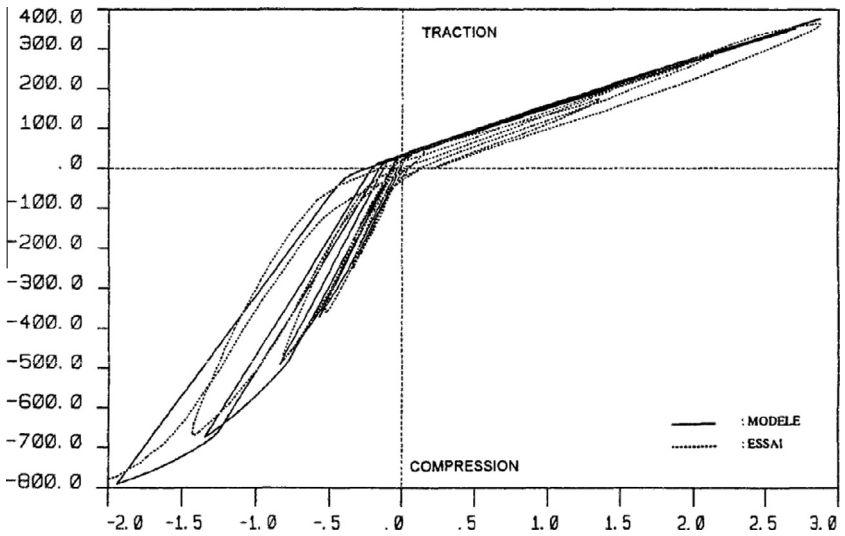

Fig. 1-1. Experimental results of a RC column under alternated tension–compression loadings (from Benmansour, 1997): axial stress resultant (in kN) versus axial strain.

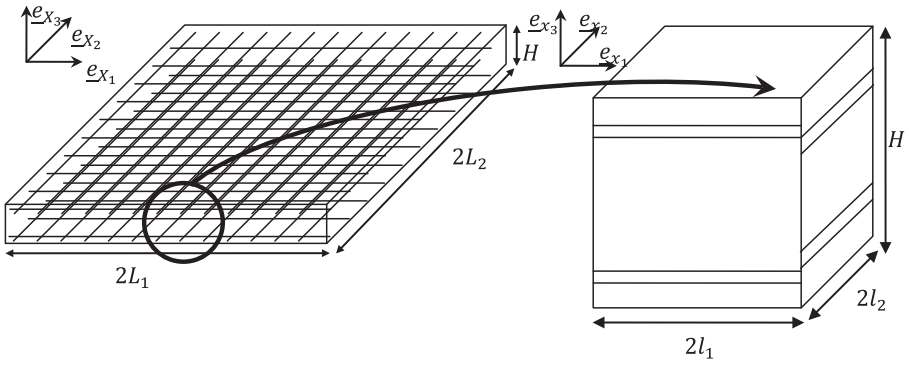

Fig. 2-1. RVE **Ω** definition from the actual RC plate geometry.

characteristic geometrical dimensions. Though this estimated value has to be reduced due to the actual finite thickness of the considered RC sections, the result remains true, i.e. we are funded to keep this assumption in the following.

The assumed interfacial displacement jump has only one tangential component: we do not consider any normal separation between steel and concrete. Moreover, we do not consider any elastic displacement jump.

Bond strength (cohesion between steel bar and surrounding concrete) can be defined according the CEB-FIP Model Code 1990 (1993), while for the sake of simplicity, we assume that there is no slip before reaching the bond strength, which is conventionally correlated to the compressive concrete strength σ_c' by: $\tau_{max} = 2.5(\sigma_c')^{1/2}$, with σ_c' expressed in MPa, for confined concrete and ribbed rebar (case considered in the applications in view). However, we noticed that for large values of slip (beyond about the rib spacing of rebar), the bond strength τ_{max} can be reduced by a factor 0.4. Moreover, it has been reported that the cyclic loading causes a quite significant deteriorated friction resistance due to crushing of concrete in the vicinity of the bar ribs (Murcia-Delso et al., 2011). Nevertheless, as the maximum value of slip occurs in concrete macro-crack, whose width is generally lower than the rib spacing, we decided to restrict to the original τ_{max} value. We also decided to ignore the dependency of the bond strength on steel stress state (tension or compression) as recognised by several authors (Feenstra and De Borst, 1996).

Unlike proposed in many previous works, such as Chaboche (2003), Melo et al. (2011) and Nedjar (2001), our modelling assumptions lead to a definition of an elastic strain different from the usual difference between strain tensor and "plastic strain" tensor, using a damage dependent operator applied to the "plastic strain" tensor, as shown in our previous paper by Combescure et al. (2013), justified by a closed form, which has been established in one dimension.

1.3. Outline of this work

This paper is organised as follows:

The formulation of the DHRC homogenised constitutive model refers to the general framework of a chained structural analysis method, based on a prior micro-scale analysis to the macro-scale structural analysis (Yvonnet et al., 2009), contrary to a coupled method like the multilevel finite element FE^2 (Feyel, 1999), which is expected to induce a heavy computational burden for the range of applications in view.

A periodic homogenisation approach by averaging method, applied to plates, is implemented. The definition of the Representative Volume Element (RVE) (Caillerie and Nedelec, 1984; Destuynder and Theodory, 1986) takes advantage of steel bar grids periodicity in RC slabs and walls and of the experimentally observed periodicity of damage and debonding. One advantage is the ability to address any kind of steel bar grids geometry including, if necessary, the transverse reinforcement. Another is to get accurate results at macro-scale when the spatial distribution of loading has larger length-scale than those of the RVE.

In Section 2, we review in details the assumptions made to idealise the RVE: geometry of components, mechanical phenomena accounted for, local state variables used for the mechanical state description, and mechanical requirements such as average strain theorem, Hill–Mandel's mechanical principle (Hill, 1972) and definition of the macro-scale state variables for the homogenised RC plate constitutive model (Sanchez-Palencia et al., 1987; Suquet, 1987, 1993; Caillerie and Nedelec, 1984).

In Section 3, we describe the auxiliary problems to be solved in the RVE in order to obtain the local mechanical fields, needed to compute the macroscopic energy density of the RC plate constitutive model, and the macroscopic dissipation potentials within the framework of Generalised Standard Materials theory (Halphen and Nguyen, 1975; Sanchez-Palencia, 1980). We show that the general formulation of the homogenised nonlinear constitutive model is not directly dependent on the idealisation of the local damage and bond sliding mechanism.

In Section 4, after having given general comments about the implementation of the DHRC model in the finite element software *Code_Aster* (Code Aster, 2001), we present the numerical DHRC parameters identification procedure where the macroscopic strain energy density function and thresholds are identified from geometrical data and material mechanical properties of the RC plate.

Finally, in Section 5, we display some numerical results obtained with the DHRC constitutive model, and comparison with experimental data gathered on realistic RC structural elements and building under seismic loading.

1.4. Notations

The following notations will be adopted throughout the paper:

–First order tensors and vectors will be underlined, second order tensors will be noted in bold font and third and further order tensors will be noted with doubled letters;
–A Cartesian orthonormal coordinate system is chosen so that covariant and contra-variant components are assimilated.
–Tensor components will be given through subscripts relatively to the differential manifold used: Greek subscripts will set for integers ranging from 1 to 2 and Latin ones for integers ranging from 1 to 3.

–We will need subscripts having no tensorial sense but only aiming at distinguishing lower and upper halves of the RC plate, which will denoted by dummy Greek superscripts ρ, ζ.
–The simply contracted tensorial product will be noted by a simple dot "." and the double one by two dots ":".
–Uppercase letters will refer generally to the macroscopic scale and lowercase ones to the microscopic scale.

2. Theoretical background

2.1. Actual problem and modelling assumptions

We consider a concrete panel reinforced by two steel grids located on one side and the other of the middle plane of the plate. The thickness H of the plate is considered to be small compared to its overall lateral dimensions L_1 and L_2, see Fig. 2-1, and the grids are composed with a periodic pattern of natural periodicity along $\underline{e}_{x_1}$ and $\underline{e}_{x_2}$ directions of the same length order as H. Moreover we consider that external loading and inertia forces spatial distributions are "smooth" with respect to the thickness H of the plate and restricted to the low frequencies range, as usual for seismic studies. Thus, it is possible to define a Reference Volume Element (RVE), denoted hereafter by Ω, including both concrete and steel grids, whose lateral dimensions are l_1 and l_2, see Fig. 2-1. We assume that the ratio of the lateral dimensions l_1 or l_2 over the dimensions L_1 or L_2 of the whole plate is of the same length order as the ratio of the plate thickness H over its lateral dimensions.

We are interested in deriving an overall macroscopic plate constitutive relation and the previous geometrical characteristics lead us to use a multi-scale analysis or a homogenisation technique, as it was already proposed in the literature for many decades. In the case where components are assumed to be linear elastic, this multi-scale approach has been justified by using an asymptotic expansion method on three-dimensional elasticity equations. It leads to the well-known bi-dimensional linear Love–Kirchhoff's thin plate theory if the dimensionless size of heterogeneities is of the same order that the relative slenderness of the solid (Caillerie and Nedelec, 1984; Ciarlet, 1979; Sanchez-Palencia et al., 1987).

Both periodicity directions $\underline{e}_{X_1}$ and $\underline{e}_{X_2}$, corresponding to steel grid rebar directions, will be preferred directions for the sequel of this paper. The chosen microscopic coordinate system will be the steel grid coordinate system $(O, \underline{e}_{x_1}, \underline{e}_{x_2}, \underline{e}_{x_3})$, where $\underline{e}_{x_3} = \underline{e}_{X_3}$ and O is the centre of the considered RVE. The plane $x_3 = 0$ is the mid-plane of the RVE.

Upper and lower faces of the RVE are assumed to be free of charge, see Caillerie and Nedelec (1984).

Given the fact that material considerations for the actual RC plate problem are complex, several simplifications have been proposed. As reported in Suquet's work (Suquet, 1993), the essential properties of the macroscopic homogenised model are directly defined from average energetic quantities that are computed from microscopic corresponding ones in the RVE and from some optimisation arguments associated to local thermodynamic equilibrium – especially in the standard generalised materials context (Halphen and Nguyen, 1975). Therefore, it is believed that average quantities can catch with a reasonable good agreement the overall behaviour of an actual RC plate, even if the detail of microscopic phenomena is roughly idealised. The constitutive hypothesis about materials and their bond behaviours, needed to formulate the mathematical expression of the model are listed below with their justifications.

2.1.1. Materials behaviour in RVE Ω

Hyp 1. Steel is considered linear elastic, without irreversible plastic strains, as we do not consider ultimate states of the RC plate. We denote by $\mathbb{a}^s$ the corresponding elastic tensor.

Hyp 2. Concrete is considered elastic and damageable, according to the following constitutive model $\boldsymbol{\sigma} = \mathbb{a}^c(d) : \boldsymbol{\varepsilon}, d$ being a scalar damage variable idealising distributed cracking. The associated induced anisotropy is modelled through a suitable definition of $\mathbb{a}^c(d)$. Concrete elasticity tensor $\mathbb{a}^c(d)$ is defined by its initial undamaged value $\mathbb{a}^c(0)$, whose components are reduced by a decreasing convex damage function $\xi(d)$. We will give more details about the concrete constitutive model in Section 4.2.

2.1.2. Steel–concrete interface in RVE Ω

Hyp 3. Concrete and steel rebar can slide one on the other beyond a given threshold.>

Hyp 4. The bond status at steel–concrete interface is either sticking or sliding. Normal separation is not allowed. We do not consider any interface elastic energy associated to the sliding motion.

Hyp 5. The relative steel–concrete sliding, appearing after concrete damage and transmission of internal forces from concrete to steel rebar, can occur only in the two preferred directions $\underline{e}_{x_1}$ and $\underline{e}_{x_2}$ – along longitudinal rebar. It can differ whether considering the bar of the upper grid or of the lower grid, thus allowing to take into account its consequence on the RC plate flexural behaviour. Let's denote by Γ_b the generic steel–concrete interfaces along $\underline{e}_{x_1}$ or $\underline{e}_{x_2}$.

Hyp 6. Steel rebar orthogonal to the sliding direction – i.e. either perpendicular grid rebar or transversal rebar – are considered to prevent relative sliding. As a consequence, steel–concrete sliding is periodical with a period equal to the spacing between two consecutive grid bars in the considered sliding direction. This defines the lateral dimensions of the RVE Ω.

2.1.3. Non-uniform damage in RVE Ω

Hyp 7. In order to idealise the non-uniform damage distribution of concrete along the steel rebar, concrete domain in the RVE is in fact divided into two sub-domains associated respectively to sound concrete and damaged one. Therefore, we define a whole RVE partition into two sub-domains Ω_{sd} and Ω_{dm}, respectively. Stresses and displacements are assumed to be continuous when crossing the Γ_s interface between these two sub-domains.

Actually, concrete of the plate is not damaged in a uniform way in its volume. In order to idealise this phenomenon, one should introduce a non-uniformly distributed damage variable d in the whole RVE. Nevertheless, according to the Suquet's work (Suquet, 1987), this non-uniformity of the microscopic internal variable field leads to the necessity to consider an infinite number of macroscopic internal variables at each macroscopic material point. This issue prevents the practical use of the macroscopic standard generalised model that would result from the chosen microscopic ones. However, still according to Suquet (1987), it is possible to reduce this number of internal variables to a finite one if it can

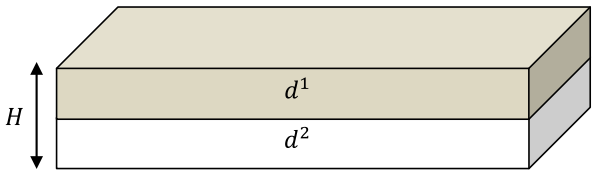

Fig. 2-2. Depiction of the microscopic damage variable **d** discretised in the RVE thickness.

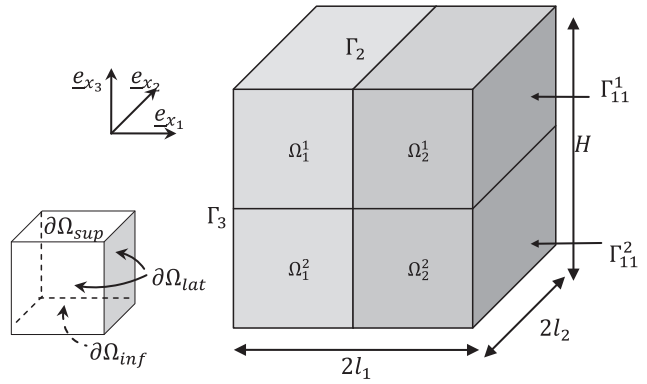

Fig. 2-3. Depiction of the sub-domains within the RVE thickness.

be demonstrated that these internal variables are uniform or piecewise uniform or more generally described by a vector space of finite dimension. The standard generalised character of the macroscopic model is obtained from the microscopic scale behaviours thanks to the usual properties of Caratheodory's functions of Convex Analysis. Thus, if such a chosen set of internal variables can represent the actual material state in the RVE, with a sufficient approximation degree, it is possible to build a macroscopic standard generalised model with a finite number of macroscopic internal variables. In our study, in order to restrict the number of macroscopic internal variables, we decided to define only one microscopic internal variable d for damage, considered as piecewise uniformly distributed inside the whole RVE and two sets of materials representing two different states of damage in concrete located in sub-domains Ω_{sd} and Ω_{dm}. This distribution of microscopic damage allows in a simple way the representation of the " tension-stiffening" effect (Combescure et al., 2013). The values of microscopic and macroscopic internal variables d and D are then equated, for the sake of simplicity, without losing any generality, since the only matter is the actual value of the respective elastic stiffness tensors.

Hyp 8. In order to take into account the *a priori* non-uniform damage in the RVE thickness, two damage variables will be set up corresponding to the piecewise damage in the upper and lower halves of the RVE:

$$d = \begin{cases} d^1 & \text{if } x_3 \geqslant 0 \\ d^2 & \text{if } x_3 < 0 \end{cases} \tag{2-1}$$

This leads to a macroscopic damage also decomposed into two macroscopic variables D^1 and D^2.

This strong hypothesis of microscopic damage variable stepped distribution is about to represent common experimental observations during four points bending tests on RC plates: cracks opened in tension parts of the plate appear and propagate dynamically quasi-instantaneously through about the half of

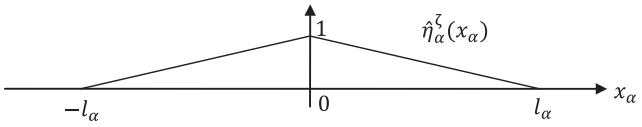

Fig. 2-4. Periodic sliding shape function distribution $\hat{\eta}_\alpha^\zeta$ along the $\underline{\mathbf{e}}_{x_\alpha}$ direction with unitary amplitude in the RVE.

thickness. This crack propagation time scale is much smaller than the one considered in seismic analysis and it is then adequate to separate damage into two variables depending on the position $\mathbf{x_3}$ in the plate thickness. The distinction between those two damage steps is chosen to be at the exact middle plane $\mathbf{\Gamma_m}$ of the plate, being the perfectly stuck interface between upper and lower halves of the RVE. This strong approximation is in accordance with reinforced concrete design standards and regulations where it is advised to consider only half of the concrete section, for bending design, e.g. CEB-FIP Model Code 1990 (1993). In the sequel, microscopic and macroscopic damage variables will be respectively noted $\mathbf{d}^\zeta$ and $\mathbf{D}^\zeta$ depending if the considered variable is the one of the upper ($\zeta = \mathbf{1}$) or lower ($\zeta = \mathbf{2}$) half of the RVE, see Fig. 2-2.

Once admitted this distinction between upper and lower halves of the RVE, sub-domains Ω_i ($i = sd, dm$, according to the damage status) and steel–concrete interfaces Γ_b must be split respectively in Ω_i^1, Ω_i^2 and $\Gamma_b^1,\ \Gamma_b^2$. Interfaces Γ_b^1 and Γ_b^2 will then be denoted by Γ_b^ζ, with $\zeta = 1, 2$.

2.1.4. Non-uniform steel–concrete debonding in RVE Ω

Let's consider, in the RVE sketched at Fig. 2-3, that sliding can occur at steel–concrete interfaces Γ_b^ζ along the $\underline{e}_{x_1}$ or $\underline{e}_{x_2}$ directions.

The shapes of sliding functions $\underline{\eta}^\zeta(\underline{x})$ at the interfaces Γ_b^ζ should result from the mechanical energy minimisation and then depends on the loading history in the RVE. Thus, they remain unknown before the introduction of macroscopic loading over the whole plate and cannot be determined *a priori*. As a consequence, the choice is made to prescribe *a priori* shapes for these functions in order to process conveniently to the periodic homogenisation with a limited number of variables. Moreover, as well as damage has been be chosen piecewise uniform inside the whole unit cell, it appears necessary to define sliding along each rebar from one only parameter per direction and per grid. Several possibilities can then be chosen: either the tangential displacement gap corresponding to the sliding is constant, either bond-stress induced by this sliding are. According to Marti et al. (1998), debonding induced stress are assumed to be piecewise constant.

Hyp 9. Considering the previous observation from Marti et al. (1998), a bilinear sliding function (sketched at Fig. 2-4) is chosen – corresponding to piecewise bond stresses at the interface Γ_b^ζ. This sliding function is only parameterised by its amplitude, its periodicity being fixed by the one of the RVE.

Hyp 10. Moreover, it will be considered that steel–concrete sliding vector in the $\underline{e}_{x_\alpha}$ direction, denoted by $\underline{\eta}_\alpha^\zeta$, depends only on the x_α coordinate: it takes the same value at any point located at the steel–concrete interface Γ_b^ζ for a given x_α. Let's denote by $\hat{\eta}_\alpha^\zeta(x_\alpha)$ the sliding function of unitary amplitude for the $\underline{e}_{x_\alpha}$ direction. As a result: $\underline{\eta}_\alpha^\zeta(x_\alpha) = E_\alpha^{\eta^\zeta}\hat{\eta}_\alpha^\zeta(x_\alpha).\underline{e}_{x_\alpha}, E_\alpha^{\eta^\zeta}$ being its amplitude. Moreover, we observe that $\frac{1}{l_\alpha}\int_{-l_\alpha}^{l_\alpha}\hat{\eta}_\alpha^\zeta dx_\alpha = 1$.

2.1.5. Overall strains measures and macroscopic state variables on RVE $\boldsymbol{\Omega}$

Now, according to the previous selection of phenomena to be idealised, we have to define a set of independent state variables, able to describe the mechanical state evolutions of the RC plate structural element at the macro-scale. First of all, the local microscopic displacement field $\underline{u}$ in the RVE $\Omega = \cup\Omega_i^\zeta$ ($i = sd, dm$ in concrete, and $i = s$ in steel rebar) is split into a regular part $\underline{u}^r$ and a discontinuous one $\underline{u}^d$, associated with the debonding relative displacement defined by the $\underline{\eta}_\alpha^\zeta$ functions Hyp (10) at the steel–concrete interfaces Γ_b^ζ.

The overall strains measures defined as the result of the homogenisation of thin plate are the following mean surface strain tensors of second order, according to Kirchhoff–Love's kinematics (Caillerie and Nedelec, 1984): macroscopic membrane strain tensor $\mathbf{E}$, whose components are denoted by $E_{\alpha\beta}$, and macroscopic bending strain tensor $\mathbf{K}$ (curvature at first order), whose components are denoted by $K_{\alpha\beta}$. As we denote by $\boldsymbol{\varepsilon}(\underline{u})$ the microscopic strain tensor associated to local displacement field $\underline{u}$ in the RVE $\Omega = \cup\Omega_i^\zeta$, the components of $\mathbf{E}$ and $\mathbf{K}$ tensors are defined by the following average linear operators from the regular part $\underline{u}^r$ of the displacement field:

$$\begin{cases} E_{\alpha\beta} = \frac{1}{|\Omega|}\int_{\cup\Omega_i^\zeta} \varepsilon_{\alpha\beta}(\underline{u}^r)d\Omega \\ K_{\alpha\beta} = \frac{12}{H^2|\Omega|}\int_{\cup\Omega_i^\zeta} -x_3\varepsilon_{\alpha\beta}(\underline{u}^r)d\Omega \end{cases} \tag{2-2}$$

In the sequel, the following notation $\langle\cdot\rangle_\Omega = \frac{1}{|\Omega|}\int_{\cup\Omega_i^\zeta}.d\Omega$ stands for the average value of the considered field in the RVE. We can easily observe that the expressions in (2-2) encompass the usual definition for homogeneous plate kinematics.

We must now deal with the non-regular part $\underline{u}^d$ of the displacement field in the RVE. In the sequel $[\![.]\!]$ stands for the jump operator on the steel–concrete interface. So, we define the macroscopic sliding strain tensor $\mathbf{E}^{\boldsymbol{\eta}^\zeta}$ as the average of sliding on each steel–concrete interface Γ_b^ζ. First, we observe that the contribution of discontinuous displacement $\underline{u}^d$ to the macroscopic strain tensors vanishes, due to Hyp 4 and 10 (Andrieux et al., 1986):

$$\frac{1}{|\Omega|}\int_{\Gamma_b^\zeta}[\![\underline{u}^d]\!]\otimes^s\underline{n}dS = 0; \quad \frac{1}{|\Omega|}\int_{\Gamma_b^\zeta}x_3.[\![\underline{u}^d]\!]\otimes^s\underline{n}dS = 0 \tag{2-3}$$

where $\underline{n}$ is the outward normal at the steel–concrete interface Γ_b^ζ and $\otimes^s$ stands for the symmetrised dyadic tensor product. According to Hyp 4, the displacement discontinuity $[\![\underline{u}^d]\!] = \underline{\eta}^\zeta(\underline{x})$ at the interface Γ_b^ζ does not include any opening or separation in the $\underline{n}$ direction, but only tangential sliding $\underline{\eta}_\alpha^\zeta$. Extending the proposed definition by Combescure et al. (2013), the components of $\mathbf{E}^{\boldsymbol{\eta}^\zeta}$ are:

$$E_{\alpha\alpha}^{\eta_\alpha^\zeta} = \frac{1}{|\Omega|}\int_{\Gamma_b^\zeta}\left([\![\underline{u}^d]\!].\underline{e}_{x_\alpha}\right).\underline{e}_{x_\alpha}\otimes^s\underline{e}_{x_\alpha}dS \tag{2-4}$$

Indeed, the only non-zero components of tensor $\mathbf{E}^{\boldsymbol{\eta}^\zeta}$ are $E_{\alpha\alpha}^{\eta_\alpha^\zeta}$. Vector $\underline{E}^{\eta^\zeta}$ will then more conveniently be considered in the following as a first-order tensor of the plate mean surface, whose components are denoted by $E_\alpha^{\eta_\alpha^\zeta}$.

The macroscopic primal state variables associated to the DHRC proposed model are then: membrane strains $\mathbf{E}$ and bending strains $\mathbf{K}$ tensors, damage variables D^ζ on upper and lower halves of the homogenised plate, sliding strain $\underline{E}^{\eta^\zeta}$ vectors on upper and lower grids. These variables will be used to define state functions, as the macroscopic free energy density $\mathcal{W}(\mathbf{E}, \mathbf{K}, D^\zeta, \underline{E}^{\eta^\zeta})$.

3. Weak form of the auxiliary problems and homogenised model

3.1. Local auxiliary problems

In order to determine the macroscopic constitutive relation, we have to establish the relation between microscopic fields and macroscopic ones, for various fixed values of internal state variables. This relation concerns displacements fields, strain work density and dissipation potentials.

At the RVE level, as a consequence of equalities (2-2) and (2-4), let's introduce two microscopic auxiliary displacement fields:

- "elastic" displacement fields in membrane $\underline{\chi}$ and bending $\underline{\xi}$, corresponding to a given non-zero macroscopic strain tensor – $\mathbf{E}$ in membrane and $\mathbf{K}$ in bending – with zero sliding ($\underline{E}^{\eta^\zeta} = \mathbf{0}$)

- "sliding" displacement fields $\underline{\chi}^{\eta_\alpha^\zeta}$, corresponding to vanishing macroscopic strains ($\mathbf{E} = \mathbf{0}, \mathbf{K} = \mathbf{0}$) corresponding to a given sliding function $\eta_\alpha^\zeta(x_\alpha)$ or equivalently a given $E_\alpha^{\eta_\alpha^\zeta}$, as done in Andrieux et al. (1986) and Pensée and Kondo (2001).

Hence the microscopic displacement field $\underline{u}$, solution of the local boundary value problem in the RVE, can be decomposed as follows (omitting intentionally the solid motion to shorten the expression):

$$\begin{cases} u_\alpha(\underline{x}) = E_{\alpha\beta}x_\beta - K_{\alpha\beta}x_\beta x_3 + E_{\beta\gamma}\chi_\alpha^{\beta\gamma}(\underline{x}) + K_{\beta\gamma}\xi_\alpha^{\beta\gamma}(\underline{x}) + E_\beta^{\eta_\alpha^\zeta}\chi_\alpha^{\eta_\beta^\zeta}(\underline{x}) \\ u_3(\underline{x}) = E_{\beta\gamma}\chi_3^{\beta\gamma}(\underline{x}) + K_{\beta\gamma}\xi_3^{\beta\gamma}(\underline{x}) + E_\beta^{\eta_\alpha^\zeta}\chi_3^{\eta_\beta^\zeta}(\underline{x}) \end{cases} \tag{3-1}$$

We define the following functional spaces for displacement fields in Ω (Caillerie and Nedelec, 1984):

$$\mathcal{U}_{ad}^0 = \left\{\underline{v}/\underline{v} \text{ periodic in } x_1 \text{ and } x_2,\ \underline{v} \text{ continuous on } \Gamma_b^1 \cup \Gamma_b^2 \cup \Gamma_s,\right\} \tag{3-2}$$

and:

$$\mathcal{U}_{ad}^{\alpha\rho} = \{\underline{v}/\underline{v} \text{ periodic in } x_1 \text{ and } x_2,\ \underline{v} \text{ continuous on } \Gamma_s, \\ v_n \text{ continuous and } [\![\underline{v}_T]\!] = \mathrm{E}_\alpha^{\eta\rho}\hat{\eta}_\alpha^\rho(x_\alpha).\underline{e}_{x_\alpha} \text{ on } \Gamma_b^\rho\} \tag{3-3}$$

Remark 1. We can easily prove that $\langle\boldsymbol{\varepsilon}(\underline{v})\rangle_\Omega = \langle x_3\boldsymbol{\varepsilon}(\underline{v})\rangle_\Omega = \mathbf{0}$ for any v in $\mathcal{U}_{ad}^0$ due to the periodicity and, using Eqs. (2-3), that $\langle\boldsymbol{\varepsilon}(\underline{v})\rangle_\Omega = \langle x_3\boldsymbol{\varepsilon}(\underline{v})\rangle_\Omega = \mathbf{0}$ for any v in $\mathcal{U}_{ad}^{\alpha\rho}$.

Strain work density at the macroscopic scale is obtained by the exploitation of extended Hill–Mandel's principle (Sanchez-Palencia et al., 1987; Suquet, 1987), extended to thin plate case by Caillerie and Nedelec (1984). Generalised stress resultants, dual of the primal overall strain variables $\boldsymbol{E}, \boldsymbol{K}$, and $\underline{E}^{\eta^\zeta}$ are respectively denoted by: $\mathbf{N}, \mathbf{M}$ and debonding stress vector $\underline{\Sigma}^{\eta^\zeta}$. Macroscopic strain work balance reads:

$$\mathbf{N}.\boldsymbol{E} + \mathbf{M}.\boldsymbol{K} + \underline{\Sigma}^{\eta^\zeta}.\underline{E}^{\eta^\zeta} = \frac{H}{|\Omega|}\int_{\cup\Omega_i^\zeta}\sigma_{pq}.\varepsilon_{pq}(\underline{u})d\Omega \tag{3-4}$$

Introducing Hyp 1 and 2 assumptions about the material behaviours within the RVE, the overall strain variables definition (cf. Section 2.1.5), and the microscopic displacement field decomposition (3-1) in the strain work balance (3-4), microscopic periodic auxiliary displacement fields satisfy the following ten linear elastic auxiliary problems, defined in the RVE, the damage state d^ζ being fixed (subscript $k = c$ or s, for concrete or steel):

Find $\underline{\chi}^{\alpha\beta} \in \mathcal{U}^0_{ad}$ so that:

$$\int_{\cup\Omega_i^\zeta} \varepsilon_{pq}\left(\underline{\chi}^{\alpha\beta}\right) \mathbb{a}^k_{pqrs}\left(d^\zeta\right) \varepsilon_{rs}(\underline{v}) d\Omega = -\int_{\cup\Omega_i^\zeta} \mathbb{a}^k_{\alpha\beta rs}\left(d^\zeta\right) \varepsilon_{rs}(\underline{v}) d\Omega \quad \forall \underline{v} \in \mathcal{U}^0_{ad}$$

Find $\underline{\xi}^{\alpha\beta} \in \mathcal{U}^0_{ad}$ so that:

$$\int_{\cup\Omega_i^\zeta} \varepsilon_{pq}\left(\underline{\xi}^{\alpha\beta}\right) \mathbb{a}^k_{pqrs}\left(d^\zeta\right) \varepsilon_{rs}(\underline{v}) d\Omega = +\int_{\cup\Omega_i^\zeta} x_3 . \mathbb{a}^k_{\alpha\beta rs}\left(d^\zeta\right) \varepsilon_{rs}(\underline{v}) d\Omega \quad \forall \underline{v} \in \mathcal{U}^0_{ad} \tag{3-5}$$

Find $\underline{\chi}^{\eta^\rho_\alpha} \in \mathcal{U}^{\alpha\rho}_{ad}$ so that:

$$\int_{\cup\Omega_i^\zeta} \varepsilon_{pq}\left(\underline{\chi}^{\eta^\rho_\alpha}\right) \mathbb{a}^k_{pqrs}\left(d^\zeta\right) \varepsilon_{rs}\left(\underline{v} - \underline{\chi}^{\eta^\rho_\alpha}\right) d\Omega = 0 \quad \forall \underline{v} \in \mathcal{U}^{\alpha\rho}_{ad} \tag{3-6}$$

i.e. three problems in membrane, three ones in bending and the last four associated to sliding. Thus, any microscopic displacement field $\underline{u}$ *can* be expressed with the help of the previous ten auxiliary fields, by linear superposition (3-1). Thanks to these results, macroscopic strain work density can be written in terms of macroscopic state variables.

3.2. Macroscopic homogenised model

In the following we shall adopt the notation: $\langle\langle\cdot\rangle\rangle_\Omega = \frac{H}{|\Omega|}\int_{\cup\Omega_i^\zeta} .d\Omega$ for the average value per plate surface unit of the considered field in the RVE Ω, H being the plate thickness, identical to the one of the RVE. The macroscopic homogenised model is obtained through the usual exploitation of extended Hill-Mandel's principle applied to get the macroscopic Helmoltz' free energy surface density $\mathcal{W}(\boldsymbol{E}, \boldsymbol{K}, D^\zeta, \underline{E}^{\eta^\zeta})$ of the plate constitutive model. This equates the average $\langle\langle w^i(\boldsymbol{\varepsilon}(\underline{u}), d^\zeta)\rangle\rangle_\Omega$ of the microscopic free energy densities in the RVE, where, accordingly to assumptions Hyp 1 and 2:

$$w^k\left(\boldsymbol{\varepsilon}(\underline{u}), d^\zeta\right) = \frac{1}{2}\boldsymbol{\varepsilon}(\underline{u}) : \mathbb{a}^k\left(d^\zeta\right) : \boldsymbol{\varepsilon}(\underline{u}) \tag{3-7}$$

with $k = c$ or s, for concrete or steel. In the following, we will omit this superscript to ease writing.

After solving of the ten elastic linear independent auxiliary problems (3-5) (in practice by numerical analysis), the macroscopic free energy density can be expressed as follows, using expressions (3-1), depending on the macroscopic strain tensors E, $\boldsymbol{K}$ and on the macroscopic damage and sliding internal variables $\boldsymbol{D}$ and $\underline{E}^\eta$, respectively, given with fixed values:

$$\begin{aligned}
2\mathcal{W}(\boldsymbol{E}, \boldsymbol{K}, \boldsymbol{D}, \underline{E}^\eta) = {} & \boldsymbol{E} : \langle\langle \mathbb{a}(d)\rangle\rangle_\Omega : \boldsymbol{E} - E_{\alpha\beta}\langle\langle \boldsymbol{\varepsilon}\left(\underline{\chi}^{\alpha\beta}\right) : \mathbb{a}(d) \\
& : \boldsymbol{\varepsilon}\left(\underline{\chi}^{\gamma\delta}\right)\rangle\rangle_\Omega E_{\gamma\delta} - 2\boldsymbol{E} : \langle\langle x_3 \cdot \mathbb{a}(d)\rangle\rangle_\Omega \\
& : \boldsymbol{K} - 2E_{\alpha\beta}\langle\langle \boldsymbol{\varepsilon}\left(\underline{\chi}^{\alpha\beta}\right) : \mathbb{a}(d) : \boldsymbol{\varepsilon}\left(\underline{\xi}^{\gamma\delta}\right)\rangle\rangle_\Omega K_{\gamma\delta} + \boldsymbol{K} \\
& : \langle\langle x_3^2 \cdot \mathbb{a}(d)\rangle\rangle_\Omega : \boldsymbol{K} - K_{\alpha\beta}\langle\langle \boldsymbol{\varepsilon}\left(\underline{\xi}^{\alpha\beta}\right) : \mathbb{a}(d) \\
& : \boldsymbol{\varepsilon}\left(\underline{\xi}^{\gamma\delta}\right)\rangle\rangle_\Omega K_{\gamma\delta} + 2\boldsymbol{E} : \langle\langle \mathbb{a}(d) \\
& : \boldsymbol{\varepsilon}\left(\underline{\chi}^{\eta^\zeta_\gamma}\right)\rangle\rangle_\Omega \underline{E}^{\eta^\zeta_\gamma} - 2\boldsymbol{K} : \langle\langle x_3 \cdot \mathbb{a}(d) \\
& : \boldsymbol{\varepsilon}\left(\underline{\chi}^{\eta^\zeta_\gamma}\right)\rangle\rangle_\Omega \underline{E}^{\eta^\zeta_\gamma} + E^{\eta\rho}_\alpha \langle\langle \boldsymbol{\varepsilon}\left(\underline{\chi}^{\eta^\rho_\alpha}\right) : \mathbb{a}(d) \\
& : \boldsymbol{\varepsilon}\left(\underline{\chi}\eta^\zeta_\gamma\right)\rangle\rangle_\Omega \underline{E}^{\eta^\zeta_\gamma}
\end{aligned} \tag{3-8}$$

Therefore, we can identify three homogenised behaviour tensors $\mathbb{A}, \mathbb{B}, \mathbf{C}$ of respectively fourth, third and second order, defined in the tangent plane of the plate as:

$$\begin{aligned}
2\mathcal{W}(\boldsymbol{E}, \boldsymbol{K}, \boldsymbol{D}, \underline{E}^\eta) = {} & \begin{pmatrix} \boldsymbol{E} \\ \boldsymbol{K} \end{pmatrix} : \begin{pmatrix} \mathbb{A}^{mm}(\boldsymbol{D}) & \mathbb{A}^{mf}(\boldsymbol{D}) \\ \mathbb{A}^{fm}(\boldsymbol{D}) & \mathbb{A}^{ff}(\boldsymbol{D}) \end{pmatrix} : \begin{pmatrix} \boldsymbol{E} \\ \boldsymbol{K} \end{pmatrix} \\
& + 2\begin{pmatrix} \boldsymbol{E} \\ \boldsymbol{K} \end{pmatrix} : \begin{pmatrix} \mathbb{B}^{m\zeta}(\boldsymbol{D}) \\ \mathbb{B}^{f\zeta}(\boldsymbol{D}) \end{pmatrix} . \underline{E}^{\eta^\zeta} + \underline{E}^{\eta\rho} . \mathbf{C}^{\rho\zeta}(\boldsymbol{D}) . \underline{E}^{\eta^\zeta}
\end{aligned} \tag{3-9}$$

in which pure membrane (mm), pure bending (ff) and membrane-bending (mf) terms are particularised:

$$\begin{aligned}
\mathbb{A}^{mm}_{\alpha\beta\gamma\delta}(\boldsymbol{D}) &= \langle\langle \mathbb{a}_{\alpha\beta\gamma\delta}(d)\rangle\rangle_\Omega - \langle\langle \varepsilon_{ij}(\underline{\chi}^{\alpha\beta}) : \mathbb{a}_{ijkl}(d) : \varepsilon_{kl}(\underline{\chi}^{\gamma\delta})\rangle\rangle_\Omega \\
&= \langle\langle \mathbb{a}_{\alpha\beta\gamma\delta}(d)\rangle\rangle_\Omega + \langle\langle \mathbb{a}_{\alpha\beta\gamma rs}(d) : \varepsilon_{rs}(\underline{\chi}^{\gamma\delta})\rangle\rangle_\Omega
\end{aligned} \tag{3-10}$$

$$\begin{aligned}
\mathbb{A}^{mf}_{\alpha\beta\gamma\delta}(\boldsymbol{D}) &= -\langle\langle x_3 . \mathbb{a}_{\alpha\beta\gamma\delta}(d)\rangle\rangle_\Omega - \langle\langle \varepsilon_{ij}(\underline{\chi}^{\alpha\beta}) : \mathbb{a}_{ijkl}(d) : \varepsilon_{kl}(\underline{\xi}^{\gamma\delta})\rangle\rangle_\Omega \\
&= \mathbb{A}^{fm}_{\alpha\beta\gamma\delta}(\boldsymbol{D}) = -\langle\langle x_3 . \mathbb{a}_{\alpha\beta\gamma\delta}(d)\rangle\rangle_\Omega + \langle\langle \mathbb{a}_{\alpha\beta rs}(d) : \varepsilon_{rs}(\underline{\xi}^{\gamma\delta})\rangle\rangle_\Omega \\
&= -\langle\langle x_3 . \mathbb{a}_{\alpha\beta\gamma\delta}(d)\rangle\rangle_\Omega + \langle\langle x_3 . \mathbb{a}_{\gamma\delta rs}(d) : \varepsilon_{rs}(\underline{\chi}^{\alpha\beta})\rangle\rangle_\Omega
\end{aligned} \tag{3-11}$$

$$\begin{aligned}
\mathbb{A}^{ff}_{\alpha\beta\gamma\delta}(\boldsymbol{D}) &= \langle\langle x_3^2 . \mathbb{a}_{\alpha\beta\gamma\delta}(d)\rangle\rangle_\Omega - \langle\langle \varepsilon_{ij}(\underline{\xi}^{\alpha\beta}) : \mathbb{a}_{ijkl}(d) : \varepsilon_{kl}(\underline{\xi}^{\gamma\delta})\rangle\rangle_\Omega \\
&= \langle\langle x_3^2 . \mathbb{a}_{\alpha\beta\gamma\delta}(d)\rangle\rangle_\Omega - \langle\langle x_3 . \mathbb{a}_{\alpha\beta rs}(d) : \varepsilon_{rs}(\underline{\xi}^{\gamma\delta})\rangle\rangle_\Omega
\end{aligned} \tag{3-12}$$

$$\mathbb{B}^{m\zeta}_{\alpha\beta\gamma}(\boldsymbol{D}) = \langle\langle \mathbb{a}_{\alpha\beta kl}(d) : \varepsilon_{kl}\left(\underline{\chi}^{\eta^\zeta_\gamma}\right)\rangle\rangle_\Omega \tag{3-13}$$

$$\mathbb{B}^{f\zeta}_{\alpha\beta\gamma}(\boldsymbol{D}) = -\langle\langle x_3 \cdot \mathbb{a}_{\alpha\beta kl}(d) : \varepsilon_{kl}\left(\underline{\chi}^{\eta^\zeta_\gamma}\right)\rangle\rangle_\Omega \tag{3-14}$$

$$C^{\rho\zeta}_{\alpha\gamma}(\boldsymbol{D}) = -\langle\langle \varepsilon_{ij}\left(\underline{\chi}^{\eta^\rho_\alpha}\right) : \mathbb{a}_{\alpha\beta kl}(d) : \varepsilon_{kl}\left(\underline{\chi}^{\eta^\zeta_\gamma}\right)\rangle\rangle_\Omega \tag{3-15}$$

Remark 2. First terms in the expressions 3-10,3-11,3-12 correspond to the mixture rule; the second terms can be equivalently expressed using the variational formulations (3-5) as reported here. Moreover, resulting from the symmetries of elastic tensor $\mathbb{a}$, we note directly from these expressions the following symmetries: $\mathbb{A}^{mm}_{\alpha\beta\gamma\delta} = \mathbb{A}^{mm}_{\gamma\delta\alpha\beta}$, $\mathbb{A}^{ff}_{\alpha\beta\gamma\delta} = \mathbb{A}^{ff}_{\gamma\delta\alpha\beta}$, $\mathbb{A}^{mf}_{\alpha\beta\gamma\delta} = \mathbb{A}^{mf}_{\gamma\delta\alpha\beta}$, $\mathbb{B}^{m\zeta}_{\alpha\beta\gamma} = \mathbb{B}^{m\zeta}_{\beta\alpha\gamma}$, $\mathbb{B}^{f\zeta}_{\alpha\beta\gamma} = \mathbb{B}^{f\zeta}_{\beta\alpha\gamma}$, $C^{\rho\rho}_{\alpha\gamma} = C^{\rho\rho}_{\gamma\alpha}$.

As expected, this free energy density $\mathcal{W}$ has major symmetry for membrane-bending terms. Moreover, it includes a coupling term *openB* between generalised strain tensors and bond sliding vectors that depends on damage and hence strongly couples both types of internal state variables (damage and sliding).

Remark 3. The free energy density (3-9) can also be written equivalently as:

$$\begin{aligned}
2\mathcal{W}(\boldsymbol{E}, \boldsymbol{K}, \boldsymbol{D}, \underline{E}^{\boldsymbol{\eta}}) = {} & \left[\begin{pmatrix} \boldsymbol{E} \\ \boldsymbol{K} \end{pmatrix} + \begin{pmatrix} \mathbb{Q}^{m\zeta}(\boldsymbol{D}) \\ \mathbb{Q}^{f\zeta}(\boldsymbol{D}) \end{pmatrix} . \underline{E}^{\eta^\zeta}\right] : \begin{pmatrix} \mathbb{A}^{mm}(\boldsymbol{D}) & \mathbb{A}^{mf}(\boldsymbol{D}) \\ \mathbb{A}^{fm}(\boldsymbol{D}) & \mathbb{A}^{ff}(\boldsymbol{D}) \end{pmatrix} \\
& : \left[\begin{pmatrix} \boldsymbol{E} \\ \boldsymbol{K} \end{pmatrix} + \begin{pmatrix} \mathbb{Q}^{m\zeta}(\boldsymbol{D}) \\ \mathbb{Q}^{f\zeta}(\boldsymbol{D}) \end{pmatrix} . \underline{E}^{\eta^\zeta}\right] + \underline{E}^{\eta\rho} . \boldsymbol{P}^{\rho\zeta}(\boldsymbol{D}) . \underline{E}^{\eta\zeta}
\end{aligned} \tag{3-16}$$

where: $\mathbb{Q}^\zeta(\boldsymbol{D}) = \mathbb{A}^{-1}(\boldsymbol{D}) : \mathbb{B}^\zeta(\boldsymbol{D})$ and $\boldsymbol{P}^{\rho\zeta}(\boldsymbol{D}) = \boldsymbol{C}^{\rho\zeta}(\boldsymbol{D}) - \mathbb{B}^{\rho^T}(\boldsymbol{D}) : \mathbb{A}^{-1}(\boldsymbol{D}) : \mathbb{B}^\zeta(\boldsymbol{D})$.

This expression emphasises the existence in the presented free energy density of a coupling term between damage and sliding through an inelastic strain $\boldsymbol{E}^{IR}(\boldsymbol{D}) = \left(\frac{\mathbb{Q}^{m\zeta}(\boldsymbol{D})}{\mathbb{Q}^{f\zeta}(\boldsymbol{D})}\right) . \underline{E}^{\eta^\zeta}$ depending on damage variables. As observed in Combescure et al. (2013), this constitutes a feature that is justified by the homogenisation procedure from microscopic constitutive behaviour. It makes this model differ from usual constitutive models coupling damage and plasticity (Nedjar, 2001; Chaboche, 2003; Krätzig and Pölling,

2004; Shao et al., 2006; Richard and Ragueneau, 2013...) where it is more common to refer to an inelastic residual strain $\boldsymbol{E}^{IR}$ independent of damage. Conversely, the present feature can be found in the work of Andrieux et al. (1986), for the same reason, through homogenisation process.

Remark 4. Expression (3-9) of the free energy density is a natural generalisation, dedicated to plate structures, of the one-dimensional formulation proposed by Combescure et al. (2013) and remembered here: $\Phi(E,D,E^{\eta}) = \frac{A(D)\cdot E^2}{2} - B(D)\cdot E\cdot E^{\eta} + \frac{C(D)\cdot E^{\eta 2}}{2}$.

Remark 5. It is possible to prove that coupling tensor $\mathbb{B}$ is equal to zero as long as the microscopic stiffness tensor $\mathbb{a}(\mathrm{d})$ is identical in both sub-domains Ω_{sd} and Ω_{dm}, meaning that it deals with the case where damage is uniformly distributed at microscopic scale, in the whole RVE, see Appendix A. This was observed in Combescure et al. (2013) too and confirms experimental fact concerning the tension-stiffening effect or stress transfer from rebar to concrete induced by the non-uniformity of damage distribution at local scale.

According to the theoretical framework of the Thermodynamics of Irreversible Processes, the free energy density (3-9) can be differentiated to obtain the following thermodynamic forces and state laws:

Stress resultants on the homogenised plate (membrane and bending):

$$\mathbf{N} = \frac{\partial W}{\partial \boldsymbol{E}} = \left[\mathbb{A}^{mm}(\boldsymbol{D}) \quad \mathbb{A}^{mf}(\boldsymbol{D})\right] : \begin{pmatrix}\boldsymbol{E}\\ \boldsymbol{K}\end{pmatrix} + \mathbb{B}^{m\zeta}(\boldsymbol{D}).\underline{E}^{\eta\zeta} \tag{3-17}$$

$$\mathbf{M} = \frac{\partial W}{\partial \boldsymbol{K}} = \left[\mathbb{A}^{fm}(\boldsymbol{D}) \quad \mathbb{A}^{ff}(\boldsymbol{D})\right] : \begin{pmatrix}\boldsymbol{E}\\ \boldsymbol{K}\end{pmatrix} + \mathbb{B}^{f\zeta}(\boldsymbol{D}).\underline{E}^{\eta\zeta} \tag{3-18}$$

Macroscopic energy restitution rates G^{ρ}:

$$G^{\rho} = -\frac{\partial \mathcal{W}}{\partial D^{\rho}} \tag{3-19}$$

Macroscopic debonding stress vector $\underline{\Sigma}^{\eta\zeta}$:

$$\underline{\Sigma}^{\eta\zeta} = -\frac{\partial \mathcal{W}}{\partial \underline{E}^{\eta\zeta}} = -\begin{pmatrix}\mathbb{B}^{m\zeta}(\boldsymbol{D})\\ \mathbb{B}^{f\zeta}(\boldsymbol{D})\end{pmatrix} : [\boldsymbol{E} \quad \boldsymbol{K}] - \boldsymbol{C}^{\rho\zeta}(\boldsymbol{D}).\underline{E}^{\eta\rho} \tag{3-20}$$

Now, we have to define the dissipative behaviour at the macroscopic scale from local behaviours within the RVE. Standard Generalised material theoretical framework (Halphen and Nguyen, 1975) is adopted to express pseudo-potentials of dissipation at the microscopic scale, in order to take advantage of properties from Convex Analysis. Following the work by Suquet (1987), we get the macroscopic pseudo-potentials of dissipation depending on the rates of variables $D^{\zeta}, \underline{E}^{\eta\zeta}$, by the same average principle as done for the free energy density.

Hyp 11. For the sake of simplicity, dissipative phenomena considered at the microscopic scale, within the RVE, are defined with the following threshold functions for concrete damage and steel–concrete debonding (assuming constant threshold parameters k_0 and σ_{crit}, without hardening...), and the associated normality rules. We assume that threshold positive parameter σ_{crit} is the same for all steel rebar in the RVE, whatever the bar diameter (it could be easily enhanced). Then, threshold functions read:

$$f_{d^{\zeta}}(g^{\zeta}) = g^{\zeta} - k_0 \leqslant 0 \quad \text{and} \quad f^{\alpha}_{\eta^{\zeta}}(\sigma^{\zeta}_{\alpha n}) = \left(\sigma^{\zeta}_{\alpha n}\right)^2 - \sigma^2_{crit} \leqslant 0 \tag{3-21}$$

where $g^{\zeta} = -\frac{\partial w^{\zeta}}{\partial d^{\zeta}}$ is the microscopic energy restitution rate for damaged concrete in domain Ω^{ζ}_{dm} and $\sigma^{\zeta}_{\alpha n}$ are the tangential components of microscopic stress vector $\boldsymbol{\sigma}.\underline{n}$ at the Γ^{ζ}_b interface. These threshold functions define convex reversibility domains.

Remark 6. The microscopic damage threshold function results from the chosen damage model quoted in Hyp 2 and not explicitly defined until now. The sliding threshold function results from Hyp 3 and 4.

By means of the Legendre–Fenchel's transform applied on the indicatrix functions of previously defined reversibility domains, we get the following pseudo-potentials of dissipation:

$$\varphi^{*}_{d}\left(\dot{d}^{\zeta}\right) = k_0.\left|\dot{d}^{\zeta}\right| \quad \text{and} \quad \varphi^{*\eta^{\zeta}}_{\alpha}(\dot{\eta}^{\zeta}_{\alpha}) = \sigma_{crit}.\left|\dot{\eta}^{\zeta}_{\alpha}(x_{\alpha})\right| \tag{3-22}$$

These pseudo-potentials are convex, positively homogeneous of degree one, ensuring the positivity of dissipation for any admissible rates of damage internal variables $\dot{d}^{\zeta}$ and sliding ones $\dot{\eta}^{\zeta}_{\alpha}(x_{\alpha})$ Hyp (10) at steel–concrete interfaces Γ^{ζ}_b, according to the Clausius–Duhem's inequality.

Associated flow rules corresponding to the sub-gradients of threshold functions (3-21) give the rates of damage variables in Ω^{ζ}_{dm} and sliding variables at Γ^{ζ}_b:

$$\dot{d}^{\zeta} = \dot{\lambda}_{d^{\zeta}}\frac{\partial f_{d^{\zeta}}(g^{\zeta})}{\partial g^{\zeta}} = \dot{\lambda}_{d^{\zeta}} \quad \text{and} \quad [\![\dot{u}^{\zeta}_{\alpha}]\!] = \dot{\eta}^{\zeta}_{\alpha} = \dot{\lambda}^{\alpha}_{\eta^{\zeta}}\frac{\partial f^{\alpha}_{\eta^{\zeta}}(\sigma^{\zeta}_{\alpha 3})}{\partial \sigma^{\zeta}_{\alpha n}} = 2\sigma^{\zeta}_{\alpha n}\dot{\lambda}^{\alpha}_{\eta^{\zeta}} \tag{3-23}$$

where $\dot{\lambda}_{d^{\zeta}}$ and $\dot{\lambda}^{\alpha}_{\eta^{\zeta}}$ are all positive scalars determined through the consistency condition: $\dot{f}_{d^{\zeta}} = 0$ and $\dot{f}^{\alpha}_{\eta^{\zeta}} = 0$. Therefore:

$$\dot{d}^{\zeta} = 2\frac{\left(-\boldsymbol{\varepsilon} : \mathbb{a}^{k'}\left(d^{\zeta}\right) : \dot{\boldsymbol{\varepsilon}}\right)_{+}}{\boldsymbol{\varepsilon} : \mathbb{a}^{k''}\left(d^{\zeta}\right) : \boldsymbol{\varepsilon}} \geqslant 0 \quad \text{and} \quad [\![\dot{u}^{\zeta}_{\alpha}]\!] = \dot{\eta}^{\zeta}_{\alpha} = 2\sigma^{\zeta}_{\alpha n}\dot{\lambda}^{\alpha}_{\eta^{\zeta}} \geqslant 0 \tag{3-24}$$

Now, we can express dissipation pseudo-potential functions associated to macroscopic criteria (yield surfaces), being non-negative in actual evolutions and assumed to be positively homogeneous of degree one in terms of the internal variables rates, and the internal variables flow rules. According to the work of Suquet (1987) and inspired from Stolz (2010), the macroscopic mechanical intrinsic dissipation can be defined as follows:

$$\begin{aligned}\mathcal{D}\left(\dot{\boldsymbol{D}}, \dot{\underline{E}}^{\eta}\right) &= \langle\langle \boldsymbol{\sigma} : \dot{\boldsymbol{\varepsilon}}\rangle\rangle_{\Omega} - \frac{H}{|\Omega|}\int_{\Gamma^{\zeta}_b} w_{,\varepsilon}.\varepsilon_{,\eta^{\zeta}}.\dot{\underline{\eta}}^{\zeta} dS - \langle\langle \dot{w}(\boldsymbol{\varepsilon}, d^{\rho})\rangle\rangle_{\Omega}\\ &= G^{\rho}\dot{D}^{\rho} + \underline{\Sigma}^{\eta\zeta}.\dot{\underline{E}}^{\eta\zeta}\end{aligned} \tag{3-25}$$

where $w\left(\boldsymbol{\varepsilon}\left(\underline{\eta}^{\zeta}\right), d^{\rho}\right)$ is the free energy density of each material composing the RVE; let us notice that $w_{,\varepsilon}.\varepsilon_{,\eta^{\zeta}}$ designates the stress vector at the concrete-steel interface.

Remark 7. Once again, this is a generalisation, dedicated to plate structure model, of the one-dimensional formulation proposed by Combescure et al. (2013).

According to Suquet (1987), we define the macroscopic pseudo-potentials of dissipation associated to damage and bond-sliding by the average on the RVE of their microscopic corresponding expressions (3-22), and accounting for Hyp 10:

$$\Phi_d^*\left(\dot{D}^\zeta\right) = \langle\langle \varphi_d^*(\dot{d}^\zeta)\rangle\rangle_\Omega = \frac{H}{|\Omega|}\int_{\Omega^\zeta_{dm}} k_0.\left|\dot{d}^\zeta\right| d\Omega = \frac{H|\Omega^\zeta_{dm}|}{|\Omega|}k_0.\left|\dot{D}^\zeta\right| \quad \text{and}$$
$$\Phi_\alpha^{*\eta^\zeta}\left(\dot{E}_\alpha^{\eta^\zeta}\right) = \frac{H}{|\Omega|}\int_{\Gamma^\zeta_b} \varphi_\alpha^{*\eta^\zeta}(\dot{\eta}^\zeta_\alpha)dS = \frac{H}{|\Omega|}\sigma_{crit}.\left|\dot{E}_\alpha^{\eta^\zeta}\right| \int_{\Gamma^\zeta_b} \hat{\eta}^\zeta_\alpha(x_\alpha)dS = \frac{H|\Gamma^\zeta_b|}{2|\Omega|}\sigma_{crit}.\left|\dot{E}_\alpha^{\eta^\zeta}\right| \tag{3-26}$$

These convex, positively homogeneous of degree one, macroscopic pseudo-potentials of dissipation are the Legendre–Fenchel's conjugate functions of indicatrix functions of reversibility domains at the macroscopic scale. Macroscopic threshold functions can then be identified from the macroscopic mechanical intrinsic dissipation as:

$$f_{d^\rho}(G^\rho) = G^\rho - G^{\rho crit} \leqslant 0 \quad \text{and} \quad f^\alpha_{\eta^\zeta}\left(\Sigma^{\eta^\zeta}_\alpha\right) = \left(\Sigma^{\eta^\zeta}_\alpha\right)^2 - \left(\Sigma^{\zeta crit}\right)^2 \leqslant 0 \tag{3-27}$$

where the macroscopic strengths are given by:

$$G^{\zeta crit} = \frac{H|\Omega^\zeta_{dm}|}{|\Omega|}k_0 \quad \text{and} \quad \Sigma^{\zeta crit} = \frac{H|\Gamma^\zeta_b|}{2|\Omega|}\sigma_{crit} \tag{3-28}$$

Therefore, we get two damage macroscopic strengths (upper and lower halves of the RVE) and four bond sliding ones (one for each steel rebar). Finally, macroscopic flow rules take the form of normality rules, since the standard generalised properties at micro-scale are simply transferred to the macro-scale:

$$\dot{D}^\rho = \dot{\lambda}_{d^\rho}\frac{\partial f_{d^\rho}(G^\rho)}{\partial G^\rho} = \dot{\lambda}_{d^\rho} \quad \text{and} \quad \dot{E}^{\eta^\zeta}_\alpha = \dot{\lambda}^\alpha_{\eta^\zeta}\frac{\partial f^\alpha_{\eta^\zeta}(\Sigma^{\eta^\zeta}_\alpha)}{\partial \Sigma^{\eta^\zeta}_\alpha} = 2\Sigma^{\eta^\zeta}_\alpha\dot{\lambda}^\alpha_{\eta^\zeta} \tag{3-29}$$

where $\dot{\lambda}_{d^\rho}$ and $\dot{\lambda}^\alpha_{\eta^\zeta}$ are all positive scalars determined through the consistency conditions: $\dot{f}_{d^\rho} = 0$ and $\dot{f}^\alpha_{\eta^\zeta} = 0$.

Remark 8. Macroscopic threshold functions and flow rules are similar to their microscopic homonymous modulo a scaling factor. Indeed, dissipative phenomena at the microscopic scale are naturally similar to the one located at the macroscopic scale since the homogenisation process cannot create news dissipative sources (Suquet, 1987). According to the work of Suquet (1987), the considered microscopic internal damage and sliding variables being uniform or piecewise constant in the whole unit cell, one can affirm, thanks to the arguments of convex analysis, that the standard generalised properties of materials, at the microscopic scale, are transferred to the macroscopic homogenised model. Hence, the formerly presented model with its free energy density and pseudo-potentials of dissipation can be classified as a Standard Generalised model.

Remark 9. Since microscopic and macroscopic threshold functions are similar, it is possible to choose enriched threshold functions for microscopic damage and sliding. This new choice will then immediately be translated at the macroscopic scale. However, the choice of very simple threshold functions, see Hyp 11, with one only threshold parameter restricts the number of parameters to identify. Therefore, it is expected that these simple threshold functions will be sufficient for practical applications.

Remark 10. According to Remark 5, as tensor $\mathbb{B}$ vanishes if there is no damage, then $\Sigma^{\eta^\zeta}_\alpha$ vanishes too and the macroscopic bond sliding threshold cannot be reached before the macroscopic damage one.

3.2.1. Generalisation to any material with periodic internal microstructure

One should underline that some hypothesis were not used in the previous building process of the macroscopic homogenised model: these are hypothesis about damage behaviour law for concrete Hyp 2 and about the chosen shape of sliding function Hyp 10. Indeed, during the equation of homogenisation problem and the construction of the homogenised model macroscopic equations, it was never necessary to precise the damage law nor the shape of the sliding function imposed on the Γ^π_1 interfaces. In reality, both of those precisions will be needed in the parameter identification process phase. Hence hypothesis Hyp 2 and 10 will influence the auxiliary displacement fields $\underline{\chi}$, $\underline{\xi}$ and $\underline{\chi}^\eta$ and so the coefficients of the three tensors $\mathbb{A}$, $\mathbb{B}$ and $\boldsymbol{C}$, as well as their dependence on macroscopic damage variable $\boldsymbol{D}$.

As a consequence, the presented model can be generalised for any plate constituted by a material with two phases: a damageable matrix and some inclusions with geometry similar to a grid, whatever the chosen damage law for matrix and the shape of periodic sliding function imposed at the interface matrix/inclusion.

The novelty in the work presented here relies then on the closed form of the behaviour law of such a plate, through periodic homogenisation.

A free energy density of the following general form can express this behaviour law:

$$2\mathcal{W}(\boldsymbol{E}, D, \boldsymbol{E}^\eta) = \begin{pmatrix}\boldsymbol{E}\\ \boldsymbol{K}\end{pmatrix} : \begin{pmatrix}\mathbb{A}^{mm}(D) & \mathbb{A}^{mf}(D)\\ \mathbb{A}^{fm}(D) & \mathbb{A}^{ff}(D)\end{pmatrix} : \begin{pmatrix}\mathbf{E}\\ \mathbf{K}\end{pmatrix} + 2\begin{pmatrix}\boldsymbol{E}\\ \boldsymbol{K}\end{pmatrix} : \begin{pmatrix}\mathbb{B}^{\pi^m}(D)\\ \mathbb{B}^{\pi^f}(D)\end{pmatrix} : \underline{E}^{\eta\pi} + \underline{E}^{\eta\rho}.\boldsymbol{C}^{\rho\pi}(D).\underline{E}^{\eta\pi}$$

The coupling term $\mathbb{B}(\boldsymbol{D})$ can be found, under another form, in the work of Michel (1984) and Andrieux et al. (1986). Considering a plastic or micro-cracked microscopic material both teams proved that the macroscopic homogenised free energy density includes a coupling term between macroscopic strain and microscopic plastic strain, this last term depends on the microscopic stiffness tensor.

Remark 11. The study presented in this paper proves the general existence of a coupling term $\mathbb{B}(\boldsymbol{D})$. In the particular case of a constant sliding on Γ^ζ_b, then comes $\mathbb{B}(\boldsymbol{D}) = \mathbb{A} : \mathbb{I}_3$, where $\mathbb{I}_3$ is the identity third order tensor. This particular case corresponds to the usual formulations for plasticity, where macroscopic free energy can then be expressed as: $2W = \left(\boldsymbol{E} - \boldsymbol{E}^{\boldsymbol{P}}\right) : \mathbb{A}(\boldsymbol{D}) : \left(\boldsymbol{E} - \boldsymbol{E}^{\P}\right)$, with a plastic strain $\boldsymbol{E}^P = \mathbb{I}_3.\underline{E}^\eta$.

4. Finite element implementation and parameter identification

4.1. Finite element implementation

The non-linear DHRC constitutive model formulated for plate structural element has been implemented for a DKT-CST plate finite element family (Batoz, 1982), allowing a rather efficient and versatile modelling of complex building geometries.

The numerical integration of DHRC constitutive model lies on direct implicit time discretisation method (Nguyen, 1977; Simo and Taylor, 1985), which is included in the Newton' method with an elastic predictor step followed by a "plastic" corrector step, at the global balance equations stage.

4.2. Parameter identification procedure

We present in this section the general approach carried out in order to identify DHRC parameters. The needed microscopic scale

data: geometry and material characteristics, and the main steps of the proposed automated procedure are detailed.

4.2.1. Identification approach

The main difficulty to be overcome hereafter is to ensure that with a limited number of auxiliary problems solutions, we will be able to identify DHRC parameters that:

- cover the space of macroscopic states $(\boldsymbol{E},\boldsymbol{K},D^{\zeta},\underline{E}^{\eta})$,
- have a generic dependency on macroscopic damage variable D^{ζ}, from the sound state, distinguishing tensile and compressive regimes,
- ensure continuity of stress resultants $(\boldsymbol{N},\boldsymbol{M},\underline{\Sigma}^{\eta})$ at each regime change,
- ensure the convexity of the macroscopic free energy density.

We decided to perform some "snapshots" of microscopic states for a limited number of selected macroscopic ones, and to entrust the task of determining the parameters dependency to D^{ζ} to a least squares method and an appropriate selected function of D^{ζ}. We recall from Combescure et al. (2013), that in one dimension, if the microscopic damage function, controlling the elastic stiffness degradation $\mathbb{a}^{c}(d)$, is expressed as $\xi(d)=\frac{\alpha+\gamma d}{\alpha+d}$ (which is decreasing convex for $\gamma\leqslant 1$) then the macroscopic one-dimensional elastic tensor A follows the same dependency and is equal to $A=A^{0}\frac{\alpha_A+\gamma_A D}{\alpha_A+D}$, with $\gamma_A\leqslant 1$, similarly for the other tensors B and C. This ensures the convexity of the resultant Helmholtz free energy function, provided that γ is not "excessively" negative.

As shown in the previous section, from the solutions of a set of auxiliary elastic problems, we have to identify the components of three tensors $\mathbb{A},\mathbb{B}$ and $\boldsymbol{C}$ with their macroscopic damage variable D^{ζ} dependency. Two macroscopic threshold values for damage and sliding need also to be determined.

Hyp 12. According to the results obtained for the macroscopic one-dimensional case (Combescure et al., 2013), we assume the generic following dependency on D^{ζ} variable of the macroscopic tensors components (the particular expression for tensor $\mathbb{B}$ resulting from Remark 6):

$$\frac{\alpha+\gamma D^{\zeta}}{\alpha+D^{\zeta}}\ \text{for tensors}\ \mathbb{A}\ \text{and}\ \boldsymbol{C}\quad;\quad\frac{\gamma D^{\zeta}}{\alpha+D^{\zeta}}\ \text{for coupling tensor}\ \mathbb{B}\tag{4-1}$$

Of course this compromise will have to be assessed by comparison of DHRC model results with available experimental data on actual RC structures and usual loading paths.

4.2.2. Microscopic material parameters in RVE $\boldsymbol{\Omega}$

According to assumptions Hyp 1, steel is considered as linear elastic (defined by its Young's modulus E_s and Poisson's ratio ν_s). Hyp 2 assumes that concrete is elastic and damageable. The latter is defined by the following constitutive model $\boldsymbol{\sigma}=\mathbb{a}^{c}(d):\boldsymbol{\varepsilon},d$ being the microscopic scalar damage variable. In particular, we have to define damage dependency of elastic constants, how to deal with tensile and compressive regimes, the relationship with usual concrete behaviour parameters, induced anisotropy and the distribution of damaged sub-domains into the RVE according to macroscopic states.

Hyp 13. Microscopic concrete elasticity tensor $\mathbb{a}^{c}(d)$ is defined by its initial sound isotropic elastic tensor $\mathbb{a}^{c}(0)$, characterised by Young's modulus E_c and Poisson's ratio ν_c. For $d>0$, the elasticity tensor components are reduced by a multiplicative decreasing convex damage function $\xi(d)$. We propose the generic mathematical expression $\xi(d)=\frac{\alpha+\gamma d}{\alpha+d}$, with $\gamma<1$ – ensuring a stiffness degradation for increasing damage d – which produces a bilinear strain–stress response for uniaxial monotonic loading paths, see Section 4.1 of Combescure et al. (2013).

Hyp 14. In order to distinguish between tensile and compressive states in concrete sub-domains we introduce a dissymmetry in $\xi(d)$. To this end, the microscopic damage function is modified through the use of a Heaviside's function $H(x)$ and then takes the following form:

$$\xi(d,x)=\frac{\alpha_{+}+\gamma_{+}d}{\alpha_{+}+d}\mathrm{H}(x)+\frac{\alpha_{-}+\gamma_{-}d}{\alpha_{-}+d}\mathrm{H}(-x)\tag{4-2}$$

This means that damage function ξ includes four parameters:

$$\begin{cases}\alpha_{+}>0,\quad\gamma_{+}\leqslant 1,\quad\text{for tension behaviour}\\ \alpha_{-}>0,\quad\gamma_{-}\leqslant 1,\quad\text{for compression behaviour}\end{cases}\tag{4-3}$$

In practice, we take $\alpha_{+}=1$ without getting out any generality, as the only consequence is to normalise the damage variable d.

The assumption of a discontinuous microscopic damage function will not cause any numerical problem due to the specific identification procedure stated in Section 4.2.1. Indeed, this procedure relies on some "snapshots" of microscopic states for a limited number of selected macroscopic ones. Thus, no evolution or cyclic loading is computed at the microscopic level.

We will then take the following set of five values of $d:\{0,0.5,2.,10.,20.\}$, considered to cover a sufficient range of damage for an accurate identification. This choice seems to be the better compromise between relative error and computing burden.

Concrete free energy density being $w(\boldsymbol{\varepsilon},d)=\frac{1}{2}\boldsymbol{\varepsilon}:\mathbb{a}^{c}(d):\boldsymbol{\varepsilon}$, we define energy release rate by $g(\boldsymbol{\varepsilon},d)=-w_{,d}(\boldsymbol{\varepsilon},d)$, and convex reversibility domain by the damage criterion with the constant threshold value k_0, see Hyp 11 and expression (3-21):

$$g(\boldsymbol{\varepsilon},d)=-\frac{1}{2}\boldsymbol{\varepsilon}:\mathbb{a}^{c}_{,d}(d):\boldsymbol{\varepsilon}\leqslant k_0\tag{4-4}$$

According to uniaxial stress–strain curves of concrete (CEB-FIP Model Code 1990, 1993), we use the usual following parameters: concrete tensile f_t and compression f_c strength values (the former being associated to a fracture energy G_f, the later to a compression strain ε_{cm}) and we assume a threshold value f_{dc} of initial damage in compression. So, assuming a multilinear regression of the experimental stress–strain curve through this concrete constitutive model, we can associate the values of $\alpha_{-},\gamma_{-},\gamma_{+}$ and k_0 with usual engineering parameters $f_t,f_c,\varepsilon_{cm},f_{dc}$. Let us consider a pure tensile uniaxial membrane stress loading case N^{t}_{11}, in the x direction, on a sound RVE, i.e. with zero-valued internal variables: indeed the problem remains linear. Thus, referring to Eqs. (3-19) and (3-28), we may express the macroscopic energy restitution rates, which is quadratic in N^{t}_{11}:

$$G^{\zeta}=-\frac{1}{2}\left(\mathbb{A}^{-1}(\boldsymbol{0}).N_{11}\right)\mathbb{A}_{,D^{\zeta}}(\boldsymbol{0}):\left(\mathbb{A}^{-1}(\boldsymbol{0}).N_{11}\right)=\hat{G}^{t\zeta}_{N_{11}}.\left(N^{t}_{11}\right)^{2}\tag{4-5}$$

In parallel, we calculate the microscopic energy restitution rate (4-4), using (3-1) to express the local strain tensor $\boldsymbol{\varepsilon}$ using the generalised strain measures $\boldsymbol{E},\boldsymbol{K}$ obtained by inverting (3-17) and (3-18) to express them from N^{t}_{11}:

$$g=-\frac{1}{2}\boldsymbol{\varepsilon}:\mathbb{a}^{c}_{,d}(\boldsymbol{0}):\boldsymbol{\varepsilon}=\hat{g}^{t}_{N_{xx}}.\left(N^{t}_{11}\right)^{2}\tag{4-6}$$

Table 4-1
Ω_i^ζ subdomains assignments according to each kind of RVE.

RVE	Loading	Damaged half	Ω_i^ζ sub-domains
Ω_X	Membrane, bending and bond sliding	$d^1 \geqslant 0,\ d^2 = 0$	For $x_3 > 0 : \Omega^1_{dm}$ for $x_1 > 0$ and Ω^1_{sd} for $x_1 < 0$ for $x_3 < 0 : \Omega^2_{sd}$
Ω_X	Membrane, bending and bond sliding	$d^1 = 0,\ d^2 \geqslant 0$	For $x_3 > 0 : \Omega^1_{sd}$ for $x_3 < 0 : \Omega^2_{dm}$ for $x_1 > 0$ and Ω^2_{sd} for $x_1 < 0$
Ω_Y	Membrane, bending and bond sliding	$d^1 \geqslant 0,\ d^2 = 0$	For $x_3 > 0 : \Omega^1_{dm}$ for $x_2 > 0$ and Ω^1_{sd} for $x_2 < 0$ for $x_3 < 0 : \Omega^2_{sd}$
Ω_Y	Membrane, bending and bond sliding	$d^1 = 0,\ d^2 \geqslant 0$	For $x_3 > 0 : \Omega^1_{sd}$ for $x_3 < 0 : \Omega^2_{dm}$ for $x_2 > 0$ and Ω^2_{sd} for $x_2 < 0$
Ω_{45°	Membrane and bending	$d^1 \geqslant 0,\ d^2 = 0$	For $x_3 > 0 : \Omega^1_{dm}$ for any x_1, x_2 ; for $x_3 < 0 : \Omega^2_{sd}$
Ω_{45°	Membrane and bending	$d^1 = 0,\ d^2 \geqslant 0$	For $x_3 > 0 : \Omega^1_{sd}$; for $x_3 < 0 : \Omega^2_{dm}$ for any x_1, x_2

Moreover, we calculate the stress tensor $\boldsymbol{\sigma} = \mathbb{a}^c(0) : \boldsymbol{\varepsilon}$ field at any point within the RVE concrete domain Ω_c^ζ, and we determine the maximum value $\hat{\sigma}_t^{max}.|N_{11}^t|$ of the eigen-values of this tensor, according to a Rankine criterion. Equating with the given f_t parameter, we get the critical value $\tilde{N}_{11}^t$ in tension, then the following relation, see also (3-28):

$$\left(\tilde{N}_{11}^t\right)^2 = \left(\frac{f_t}{\hat{\sigma}_t^{max}}\right)^2 = \frac{k_0}{\hat{g}^t_{N_{11}}} = \frac{k_0}{\hat{G}^{t\zeta}_{N_{11}}} \frac{H|\Omega^\zeta_{dm}|}{|\Omega|} \tag{4-7}$$

Therefore, we can deduce the value of k_0 from $f_t, \hat{g}_{N_{11}^t}$ and $\hat{\sigma}_t^{max}$. We could easily proceed in the same manner for a pure compressive uniaxial membrane stress loading case N_{11}^c. Nevertheless, we assume that it is satisfactory to follow the expression shown in Section 4.2 of Combescure et al. (2013):

$$\frac{f_t^2(1-\gamma_+)}{\alpha_+} = \frac{f_{dc}^2(1-\gamma_-)}{\alpha_-} \tag{4-8}$$

We propose to roughly approximate the post-elastic part of the concrete uniaxial compression curve by a linear segment ranging from the first damage threshold f_{dc} to the extremum (ε_{cm}, f_c), so that γ_-, belonging to $]0,1]$. Then:

$$\gamma_- = \frac{|f_c - f_{dc}|}{|E_c\varepsilon_{cm} - f_{dc}|} \tag{4-9}$$

Hyp 15. Finally, we propose to choose γ_+ so that the softening post-peak tensile path becomes sufficiently weak in order to avoid any softening of the homogenised response by the DHRC constitutive model. It is expected that provided that γ_+ remains close to zero, even negative, the homogenised free energy density will be strictly convex (this will be checked at the end of the identification process). So, we do not make use of G_f.

Hence, from (4-8), we get:

$$\alpha_- = \frac{f_{dc}^2(1-\gamma_-)}{f_t^2(1-\gamma_+)} \tag{4-10}$$

Hyp 16. Given the orthotropic geometry of the plate, we assume that damage induces orthorhombic behaviour, and define the nine orthorhombic elastic constants from the values of sound concrete Lamé's constants λ_c, μ_c. The principal material directions in the (x_1, x_2) plane are chosen according to the macroscopic membrane strain directions, respectively: at 0° for the case of dilatation strains or bond sliding, at 45° for the case of shear strains only. Even if this choice could appear as arbitrary, and can be replaced by another one, it is believed that it will be satisfactory for our purposes.

Hyp 17. Variable x in Eq. (4-2) is chosen to be macroscopic membrane strain component $E_{\alpha\beta}$ for the diagonal terms of tensors $\mathbb{A}, \mathbb{B}$ and $\boldsymbol{C}$ and tensor invariant tr$\boldsymbol{E}$ for their off-diagonal terms. Therefore we are neglecting the microscopic correctors influence in the damaged elastic tensor microscopic values. Moreover, this choice keeps the needed symmetry properties of homogenised tensors $\mathbb{A}, \mathbb{B}$ and $\boldsymbol{C}$. For bending auxiliary problems, we replace tensor $\boldsymbol{E}$ by tensor $\boldsymbol{K}$. For bond sliding auxiliary problems ($E_{\alpha\beta} = 0, K_{\alpha\beta} = 0$, see Eq. (3-6)) tensile damage is expected in the considered concrete sub-domain of the RVE, thus parameter γ_+ is used.

Consequently, we set:

$$\lambda_+(d) = \lambda_c \frac{\alpha_+ + \gamma_+ d}{\alpha_+ + d};\quad \lambda_-(d) = \lambda_c \frac{\alpha_- + \gamma_- d}{\alpha_- + d};\quad \mu_+(d) = \mu_c \frac{\alpha_+ + \gamma_+ d}{\alpha_+ + d};\quad \mu_-(d) = \mu_c \frac{\alpha_- + \gamma_- d}{\alpha_- + d} \tag{4-11}$$

For bond sliding auxiliary problems, the orthorhombic elastic constants are:

$$E_1 = E_2 = \mu_+ \frac{3\lambda_+ + 2\mu_+}{\lambda_+ + \mu_+};\quad E_3 = \mu_- \frac{3\lambda_+ + 2\mu_-}{\lambda_+ + \mu_-};$$
$$G_{12} = \mu_+;\quad G_{23} = G_{31} = \mu_-;\quad \nu_{12} = \nu_{23} = \nu_{31} = \frac{\lambda_+}{2(\lambda_+ + \mu_-)} \tag{4-12}$$

Table 4-2
RVE assignments according to unitary macroscopic loading (membrane, bond sliding).

RVE Ω_X	RVE Ω_Y	RVE Ω_{45°
Macroscopic membrane strain	Macroscopic membrane strain	Macroscopic membrane strain
$E_{11} = -1,\ E_{22} = 0,\ E_{12} = 0$	$E_{11} = 1,\ E_{22} = 0,\ E_{12} = 0$	$E_{11} = 0,\ E_{22} = -1,\ E_{12} = 0$
$E_{11} = 0,\ E_{22} = 1,\ E_{12} = 0$	$E_{11} = 0,\ E_{22} = 0,\ E_{12} = 0.5$	$E_{11} = -1,\ E_{22} = 0,\ E_{12} = 0$
$E_{11} = 1,\ E_{22} = 0,\ E_{12} = 0$	$E_{11} = 0,\ E_{22} = -1,\ E_{12} = 0$	$E_{11} = 0,\ E_{22} = 1,\ E_{12} = 0$
$E_{11} = 0,\ E_{22} = 0,\ E_{12} = 0.5$	$E_{11} = -1,\ E_{22} = 0,\ E_{12} = 0$	$E_{11} = 1,\ E_{22} = 0,\ E_{12} = 0$
$E_{11} = 0,\ E_{22} = -1,\ E_{12} = 0$	$E_{11} = 0,\ E_{22} = 1,\ E_{12} = 0$	$E_{11} = 0,\ E_{22} = 0,\ E_{12} = 0.5$
Bond sliding	Bond sliding	No bond sliding
$E_1^{\eta 1} = 1$, other zero	$E_2^{\eta 1} = 1$, other zero	–
$E_1^{\eta 2} = 1$, other zero	$E_2^{\eta 2} = 1$, other zero	
$E_1^{\eta 1} = 1$, other zero	$E_2^{\eta 1} = 1$, other zero	
$E_1^{\eta 2} = 1$, other zero	$E_2^{\eta 2} = 1$, other zero	

For macroscopic membrane and bending auxiliary problems (3–5), they fulfil:

$$\begin{aligned}
&\text{If } E_{12}>0 \text{ or } K_{12}>0 \text{ then } G_{12}=\mu_+ \text{ else } G_{12}=\mu_-;\\
&\text{If } E_{11}+E_{22}>0 \text{ or } K_{11}+K_{22}+K_{12}>0 \text{ then we set}\\
&G_{12}=\mu_+;\ \ \tilde{\lambda}=\lambda_+;\ \ E_1=\mu_+\frac{3\tilde{\lambda}+2\mu_+}{\tilde{\lambda}+\mu_+};\ \ E_2=\mu_+\frac{3\tilde{\lambda}+2\mu_+}{\tilde{\lambda}+\mu_+}\\
&\text{else } G_{12}=\mu_-;\ \ \tilde{\lambda}=\lambda_-;\ \ E_1=\mu_-\frac{3\tilde{\lambda}+2\mu_-}{\tilde{\lambda}+\mu_-};\\
&\text{If } E_{22}>0 \text{ or } K_{22}>0 \text{ then } E_2=\mu_+\frac{3\tilde{\lambda}+2\mu_+}{\tilde{\lambda}+\mu_+} \text{ else } E_2=\mu_-\frac{3\tilde{\lambda}+2\mu_-}{\tilde{\lambda}+\mu_-}\\
&\text{Then } E_3=\mu_-\frac{3\tilde{\lambda}+2\mu_-}{\tilde{\lambda}+\mu_-};\ \ G_{23}=G_{31}=\mu_-;\ \ \nu_{12}=\nu_{23}=\nu_{31}=\frac{\tilde{\lambda}}{2\left(\tilde{\lambda}+\mu_-\right)}
\end{aligned} \tag{4-13}$$

Remark 12. Therefore, in pure shear strain case, compressive elastic constant $\tilde{\lambda}=\lambda_-$ is assigned.

Hyp 18. Finally, we assume several distributions of concrete sub-domains within the RVE, according to the needed dissymmetry of damage distribution (Hyp 7, 8 and 10). Hence we will consider the following three kinds of distributions of $\mathbf{\Omega}_{\mathbf{i}}^{\zeta}$ sub-domains ($\boldsymbol{i}=\boldsymbol{sd},\boldsymbol{dm}$) for sound or damaged concrete in upper or lower halves of the RVE ($\zeta=\mathbf{1},\mathbf{2}$), with previous isotropic elastic constants in the sound concrete $\mathbf{\Omega}_{\boldsymbol{sd}}^{\zeta}$ sub-domains and orthotropic elastic constants (for five damage values taken in the set: $\{\mathbf{0},\mathbf{0.5},\mathbf{2}.,\mathbf{10}.,\mathbf{20}.\}$; we performed a sensitivity analysis whose conclusion showed that it is a good compromise) and principal material directions in the damaged $\mathbf{\Omega}_{\boldsymbol{dm}}^{\zeta}$ sub-domains. These distributions constitute three kinds of RVE, named hereafter $\mathbf{\Omega_X}$ (see Fig. 2-3), and Ω_Y (first principal material direction at 0° in the (x_1,x_2) plane), $\Omega_{45°}$ (first principal material direction at 45° in the (x_1,x_2) plane), see Table 4-1.

These three kinds of RVE are designed to deal with the respective directions of macroscopic loading. The $\Omega_{45°}$ RVE is used for the shear strains loading cases, where no separation in the (x_1,x_2) plane is needed. So, in those cases the contribution of bond sliding vanishes, as we can deduce from the corresponding auxiliary problems. Conversely, as we need to perform cross products between corrector fields to determine the off-diagonal components of the homogenised tensors $\mathbb{A},\mathbb{B},\boldsymbol{C}$, we have to carry out calculations on the three kinds of RVEs for membrane and bending macroscopic strains.

Remark 13. Note that the volume of damaged concrete sub-domains is 1/4 of total for both Ω_X, Ω_Y RVEs and 1/2 of total for $\Omega_{45°}$ RVE.

Finally, we have to solve 207 auxiliary problems: nine damage $\left(d^1,d^2\right)$ values combinations (with five d^{ζ} values taken in the set: $\{0,0.5,2.,10.,20.\}$) times twenty-three kinds of RVE Ω_i^{ζ} sub-domains distributions and loading conditions: nine with the Ω_X RVE according to the x_1 direction (five without bond sliding, four with sliding conditions), nine with the Ω_Y RVE according to the x_2 direction, five with the $\Omega_{45°}$ RVE with orthotropic reference frame rotated 45° (without bond sliding). The following Table 4-2 sums up these cases; it is relevant also for pure macroscopic bending loading cases ($K_{\alpha\beta}$ instead of $E_{\alpha\beta}$), adding so fifteen times nine (135) other elastic problems to solve.

4.2.3. Macroscopic material parameters to be determined

After solving the 342 auxiliary problems, we have at our disposal enough information on the corrector fields $\underline{\chi}^{\alpha\beta}$ in membrane, $\underline{\xi}^{\alpha\beta}$ in bending and $\underline{\chi}^{\eta_\alpha^\rho}$ for bond sliding to compute the $\mathbb{A},\mathbb{B},\boldsymbol{C}$ macroscopic tensors components, see Section 3.2. All components are expressed in the reference frame determined by the steel bar grids.

Tensor $\mathbb{A}$:

Tensor $\mathbb{A}$ is the stiffness elastic damageable tensor of the homogenised RC plate tensor, see Eqs. 3-11, 3-12, 3-13. It is a symmetric fourth order tensor of the tangent plane (see Remark 3) comprising membrane, bending and coupling terms. It is possible to store it using Voigt's notation for tensors components in the reference frame of steel rebar grids, by means of 3×3 matrices:

$$\mathbb{A}=\begin{bmatrix}\mathbb{A}^{mm} & \mathbb{A}^{mf}\\ \mathbb{A}^{fm} & \mathbb{A}^{ff}\end{bmatrix} \text{ where } \mathbb{A}^{mf}=\mathbb{A}^{fm} \tag{4-14}$$

From Eqs. 3-11, 3-12, 3-13, and (3-4), we deduce that $\mathbb{A}^{mm}$ and $\mathbb{A}^{ff}$ matrices are symmetric, whereas in general no symmetry argument hold for $\mathbb{A}^{mf}$ matrix. Therefore we have $21=6+6+9$ components to be determined for tensor $\mathbb{A}$.

Remark 14. If the RC plate presents mirror symmetry (symmetry around the medium plane), then both membrane-bending coupling matrices $\mathbb{A}^{mf}$ and $\mathbb{A}^{fm}$ should vanish as long as damage variables verify $D^1=D^2$.

Hyp 19. We define the parameters α^{A} and γ^{A} characterising the dependency on macroscopic damage variable D^{ζ} Hyp (12) and the tensile/compressive distinction in membrane or positive/negative curvature in bending of the tensor $\mathbb{A}$ components Hyp (14) by:

$$\begin{aligned}
\mathbb{A}^{\zeta\tau\tau}_{\beta\delta\lambda\mu}(\boldsymbol{D},\mathrm{x})&=\frac{1}{2}\mathbb{A}^{0\tau\tau}_{\beta\delta\lambda\mu}\left(\frac{\alpha^{\mathrm{A}\zeta\tau\tau1}_{\beta\delta\lambda\mu}+\gamma^{\mathrm{A}\zeta\tau\tau1}_{\beta\delta\lambda\mu}D^1}{\alpha^{\mathrm{A}\zeta\tau\tau1}_{\beta\delta\lambda\mu}+D^1}+\frac{\alpha^{\mathrm{A}\zeta\tau\tau2}_{\beta\delta\lambda\mu}+\gamma^{\mathrm{A}\zeta\tau\tau2}_{\beta\delta\lambda\mu}D^2}{\alpha^{\mathrm{A}\zeta\tau\tau2}_{\beta\delta\lambda\mu}+D^2}\right)\mathrm{H}(\pm x)\\
\mathbb{A}^{mf}_{\beta\delta\lambda\mu}(\boldsymbol{D})&=\mathbb{A}^{0mf}_{\beta\delta\lambda\mu}+\frac{1}{2}\left(\frac{\gamma^{Amf1}_{\beta\delta\lambda\mu}D^1}{\alpha^{Amf1}_{\beta\delta\lambda\mu}+D^1}+\frac{\gamma^{Amf2}_{\beta\delta\lambda\mu}D^2}{\alpha^{Amf2}_{\beta\delta\lambda\mu}+D^2}\right)\mathrm{H}(\pm x)
\end{aligned} \tag{4-15}$$

where the superscripts $\tau\tau$ stand for membrane or bending (mm or ff), the superscript ς stands for tension or compression case and tensorial subscripts β,δ,λ,μ stand for directions in the plate tangent plane. $\mathrm{H}(\pm x)$ is the Heaviside function distinguishing tension or compression status applied to $\mathrm{x}=E_{\beta\delta}$ if $\beta\delta=\lambda\mu$ else $\mathrm{x}=det\,\mathbf{E}$. The $\mathbb{A}^{0\tau\tau}_{\beta\delta\lambda\mu}$ and $\mathbb{A}^{0mf}_{\beta\delta\lambda\mu}$ components correspond to the sound concrete homogenised elasticity. $\mathbb{A}^{0mf}_{\beta\delta\lambda\mu}$ is expected to vanish in the case of mirror symmetry, as said before. That is why we decided to adopt the particular dependency on D^{ζ} for the $\mathbb{A}^{mf}_{\beta\delta\lambda\mu}$ terms, see Eq. (4-15).

Remark 15. This special choice of x as Heaviside variable allows us to use the direct component of the strain tensor for diagonal terms and an invariant for off-diagonal ones, conserving then the symmetry of tensor $\mathbb{A}$. The Heaviside function distinguishing tensile or compressive status being not defined when $\boldsymbol{E}=\mathbf{0}$ (resp. $\boldsymbol{K}=\mathbf{0}$), arbitrarily, tension parameters are affected to the zero macroscopic strain case.

Therefore, there is a total of $21\times(1+2\times4)=189$ necessary parameters $\mathbb{A}^0_{\beta\delta\lambda\mu}$, α^{A} and γ^{A} to fully determine the elastic stiffness tensor $\mathbb{A}$, comprising its dissymmetric dependency on macroscopic damage variables D^1 and D^2 and on tensile or compressive status.

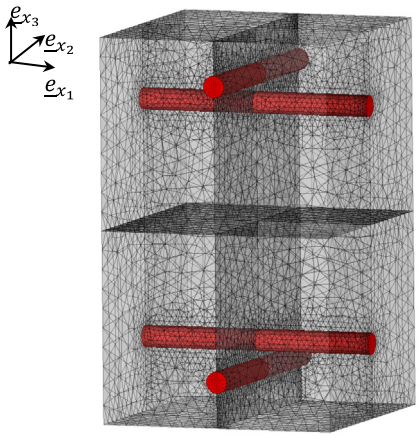

Fig. 4-1. Example of a RVE mesh for parameters identification (red: steel rebar, grey: concrete) (For interpretation of the references to color in this figure legend, the reader is referred to the web version of this article.).

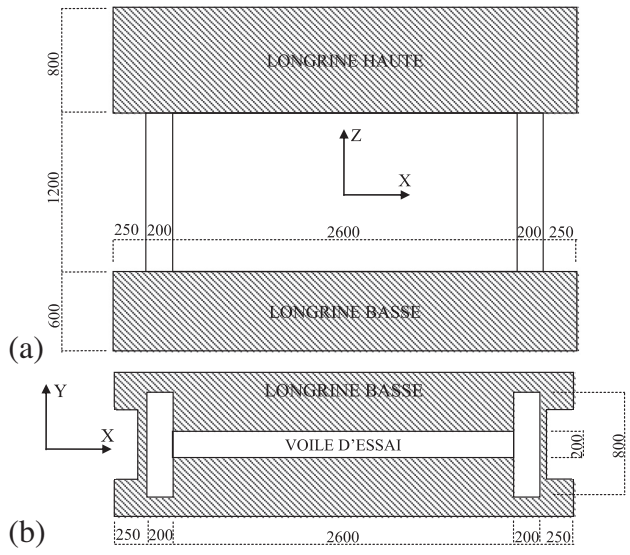

Fig. 5-1. Wall T5 with strengthening walls (length in mm): (a) elevation view, (b) bottom view.

Tensor $\mathbb{B}$: Tensor $\mathbb{B}$ is the coupling elastic damage-sliding tensor, see Eqs. (3-13) and (3-14). It is a symmetric third order tensor of the tangent plane, comprising membrane and bending terms. It is possible to store its components using Voigt's notation: $\mathbb{B} = \begin{bmatrix} \mathbb{B}^{m\zeta} \\ \mathbb{B}^{f\zeta} \end{bmatrix}$, where superscript ζ stands for sliding in the upper ($\zeta = 1$) or lower ($\zeta = 2$) grid.

Remark 16. While elastic membrane, and bending corrector fields have been computed for both tensile and compressive macroscopic loading, elastic corrector fields $\underline{\chi}^{\eta\zeta}$ are obtained for sliding displacement with zero membrane and bending macroscopic loading. Hence tensor $\mathbb{B}$ should include a tension–compression dissymmetry. However, this could introduce a discontinuity in the expression of generalised stresses as soon as macroscopic sliding strain becomes non-zero, see Eqs. (3-17), (3-18) and (3-20). Therefore, we decided to introduce no tension–compression dissymmetry in tensor $\mathbb{B}$, see Eq. (4-16).

Hyp 20. Parameters α^{B} and γ^{B} characterising the dependency on the macroscopic damage D^{ζ} Hyp (12) without tensile/compressive distinction are defined. According to Remark 6, when materials are symmetric relative to the plane Γ_s normal to the sliding bar at point O then tensor $\mathbb{B}$ components vanish, see Appendix A. As a consequence, there is no need to determine "elastic" properties for this tensor. Thus we state:

$$\mathbb{B}^{\tau\zeta}_{\beta\delta\lambda}(\boldsymbol{D}) = \frac{\gamma^{B\tau\zeta 1}_{\beta\delta\lambda} D^1}{\alpha^{B\tau\zeta 1}_{\beta\delta\lambda} + D^1} + \frac{\gamma^{B\tau\zeta 2}_{\beta\delta\lambda} D^2}{\alpha^{B\tau\zeta 2}_{\beta\delta\lambda} + D^2} \tag{4-16}$$

where the superscript τ stands for membrane or bending (m or f), the superscript ζ stands for the zone where sliding takes place (upper or lower), tensorial subscripts β, δ stand for membrane or bending directions in the plate tangent plane while tensorial subscript λ stands for sliding strain $E^{\eta\zeta}_{\lambda}$. There is, with a fixed sliding zone, 6 components for tensors $\mathbb{B}^{m\zeta}$ and $\mathbb{B}^{f\zeta}$ so 24 components for the whole tensor $\mathbb{B}$. Therefore, there is a total of $24 \times (2 \times 2) = 96$ necessary α^{B} and γ^{B} parameters to fully determine the coupling elastic damage-sliding tensor $\mathbb{B}$.

Tensor $\boldsymbol{C}$:

Tensor $\boldsymbol{C}$ is the sliding elastic "stiffness" tensor, computed from the four $\underline{\chi}^{\eta\rho}$ sliding auxiliary fields, see Eq. (3-15). It is a second order symmetric tensor of the tangent plane of the plate: $C^{\rho\zeta}_{\lambda\mu} = C^{\rho\zeta}_{\mu\lambda}$ (Remark 3). It is possible to store $\boldsymbol{C}$ components using Voigt's notation. The number of components of tensor $\boldsymbol{C}$ is then 10: sliding along $x_1 : C^{11}_{11}, C^{22}_{11}, C^{12}_{11}$, sliding along $x_2 : C^{11}_{22}, C^{22}_{22}, C^{12}_{22}$, cross terms: $C^{11}_{12}, C^{22}_{12}, C^{12}_{12}, C^{21}_{12}$.

Remark 17. As elastic $\underline{\chi}^{\eta\zeta}$ corrector fields are obtained for sliding displacements with zero membrane and bending macroscopic loading, the tensor $\boldsymbol{C}$ does not include any tension–compression dissymmetry.

Hyp 21. We define the parameters α^{C} and γ^{C} characterising the dependency on macroscopic damage D^{ζ} Hyp (12) of the tensor $\boldsymbol{C}$ components, without tensile/compressive distinction, by:

$$\boldsymbol{C}^{\rho\zeta}_{\lambda\mu}(\boldsymbol{D}) = \frac{1}{2}\boldsymbol{C}^{0\rho\zeta}_{\lambda\mu}\left(\frac{\alpha^{C\zeta 1}_{\lambda\mu} + \gamma^{C\zeta 1}_{\lambda\mu} D^1}{\alpha^{C\zeta 1}_{\lambda\mu} + D^1} + \frac{\alpha^{C\zeta 2}_{\lambda\mu} + \gamma^{C\zeta 2}_{\lambda\mu} D^2}{\alpha^{C\zeta 2}_{\lambda\mu} + D^2}\right) \tag{4-17}$$

where the superscripts ρ, ζ stand for the zones where sliding take place (upper or lower grid), tensorial subscripts λ, μ stands for sliding strain $E^{\eta\rho}_{\lambda}$ and $E^{\eta\zeta}_{\mu}$ directions in the plate tangent plane. Therefore, accounting for the symmetry of this tensor, there is a total of $10 \times (1 + 2 \times 2) = 50$ necessary $\boldsymbol{C}^{0\rho\zeta}_{\lambda\mu}, \alpha^{C}$ and γ^{C} parameters to fully determine the sliding elastic "stiffness" tensor $\boldsymbol{C}$.

To sum up, we need to identify 335 parameters after linear FEM RVE calculations:

- 21 upper diagonal terms $\mathbb{A}^{0}_{\beta\delta\lambda\mu}$ for the fourth order symmetric sound elastic plate tensor (membrane plus bending);
- 42 terms $\alpha^{A\zeta\tau\zeta}_{\beta\delta\lambda\mu}$ and 42 terms $\gamma^{A\zeta\tau\zeta}_{\beta\delta\lambda\mu}$ in the traction domain and the same number for the compression domain, describing the dependency of tensor A on damage D^{ζ},
- 48 terms $\alpha^{B\zeta\zeta}_{\beta\delta\lambda}$ and 48 terms $\gamma^{B\zeta\zeta}_{\beta\delta\lambda}$ describing the dependency of tensor B on damage D^{ζ},
- 10 upper diagonal terms $\mathbf{C}^{0\zeta}_{\beta\delta}$ for the second order symmetric sliding tensor,
- 20 terms $\alpha^{C\zeta\rho}_{\beta\delta}$ and 20 terms $\gamma^{C\zeta\rho}_{\beta\delta}$ describing the dependency of tensor $\mathbf{C}$ on damage D^{ζ}.

Table 5-1
tension and compression strength for concrete in SAFE tests (wall T5)

Evènement	Date	Mesure
Coulage	24/02/1997	
Rupture en compression (cube 150 mm d'arête)	16/07/1998	37.3 MPa
		39.9 MPa
Rupture en compression (cylindre ∅ = 6.4 mm, H = 15 cm)	16/07/1998	32.2 MPa
		29.1 MPa
Rupture en traction (cylindre ∅ = 6.4 mm, H = 15 cm)	16/07/1998	4.91 MPa
		4.73 MPa

Remark 18. In practice, due to the isotropy of undamaged concrete and the symmetry in plane x_1, x_2 of the steel rebar in the RVE, this amount of parameters can be reduced to 249. Indeed, in that case eight components $\langle\langle \mathbb{a}^k_{\alpha\beta\gamma\delta}\rangle\rangle_\Omega$ vanish, since $\mathbb{a}^k_{1112} = 0$ and so on, and we can prove from auxiliary problems (3-5) and (3-6) that the corresponding cross-product averages (e.g. $\langle\langle \varepsilon_{i,j}(\underline{\chi}^{11}) : \mathbb{a}^k_{ijkl}(d) : \varepsilon_{kl}(\underline{\chi}^{12})\rangle\rangle_\Omega$) vanish too. So, eight of $\mathbb{A}^0_{\beta\delta\lambda\mu}$ components vanish (e.g. $\mathbb{A}^0_{1112}$). As far as that goes, eight of γ^B parameters (e.g. γ^{Bm11}_{121}), six components of $\boldsymbol{C}^{0\zeta}_{\beta\delta}$ vanish, so this last tensor becomes diagonal.

Bond-sliding limit:

The last physical parameter to define more precisely is the bond-sliding limit σ^ζ_{crit}. Indeed an experimental value τ_{crit} is provided by usual pull-out tests, where a rebar centred in a concrete hexahedral volume is tensioned until sliding. According to Hyp 3 and 12, this value – assumed to be identical whatever the rebar – has to be adapted to the particular situation of the bond-sliding process in the RC RVE, for instance for a given pure unit tensile uniaxial membrane stress resultant $N^t_{\alpha\alpha}$, in the x_α direction. As sliding can occur only if damage is non-uniform within the RVE, see Hyp 7, we adopt a RVE Ω_α, with a prescribed d^ζ value in concrete sub-domain Ω^ζ_{dm}. From auxiliary field solutions in membrane $\underline{\chi}^{\alpha\beta}$ and bending $\underline{\xi}^{\alpha\beta}$ combined for the macroscopic strain measures $\mathbb{A}^{-1}(D^\zeta)\cdot N^t_{\alpha\alpha}$, with zero sliding ($\underline{E}^{\eta\zeta} = \underline{0}$), we can easily determine the steel stress resultant $F^\zeta_{N^t_{\alpha\alpha}}$ in the central section (at cutting Γ_s interface) of the considered bar $\Omega^{x_\alpha\zeta}_s$ in the x_α direction. Therefore, the resultant $F^\zeta_{N^t_{\alpha\alpha}}$ is a linear combination obtained from the corresponding unit contribution of each auxiliary field $\underline{\chi}^{\alpha\beta}$ in membrane, and $\underline{\xi}^{\alpha\beta}$ in bending, for the selected non-zero value of d^ζ, on RVE Ω_X and Ω_Y. As far as that goes, we calculate the corresponding $\Sigma^{\eta\zeta}_{\alpha N^t_{\alpha\alpha}}$ sliding stress, applying (3-20). From (3-28), equating with $\Sigma^{\zeta crit}_\alpha$ value defined by the σ^ζ_{crit} debonding value, we determine the critical value $\tilde{N}^t_{\alpha\alpha}$, thus the corresponding value of steel stress resultant $\tilde{F}^\zeta_{N^t_{\alpha\alpha}}$ which has to be equal to $\tau_{crit}|\Gamma^\zeta_b|/2$. Therefore, we get the bond-sliding threshold constants:

$$\sigma^\zeta_{crit} = \tau_{crit}\frac{|\Omega|}{H}\frac{\left|\Sigma^{\eta\zeta}_{\alpha N^t_{\alpha\alpha}}\right|}{\left|F^\zeta_{N^t_{\alpha\alpha}}\right|} \quad \text{then} \quad \Sigma^{\zeta crit}_\alpha = \frac{H|\Gamma^\zeta_b|}{2|\Omega|}\sigma^\zeta_{crit} = \frac{|\Gamma^\zeta_b|\cdot\left|\Sigma^{\eta\zeta}_{\alpha N^t_{\alpha\alpha}}\right|}{2\left|F^\zeta_{N^t_{\alpha\alpha}}\right|}\tau_{crit} \tag{4-18}$$

4.2.4. Automated procedure

The 342 linear elastic auxiliary problems can be easily solved by finite elements, using only 11 geometrical parameters and 10 material parameters $(E_s, \nu_s, E_c, \nu_c, f_t, f_c, f_{dc}, \varepsilon_{cm}, \tau_{crit}, \gamma_+)$ to define the whole RVE mechanical model. These parameters are in practice the ones required from practitioners to identify DHRC parameters set.

In order to make easy the parameter identification, an automated procedure has been implemented. The approximate CPU time needed is about 5 min on a usual personal computer.

Steel rebar are represented by cylinders of main axis x_1 or x_2. An example of a mesh for the numerical unit cell is presented on Fig. 4-1. The example concerns here a plate of 20 cm of thickness with a steel proportion of 0.8% and a steel rebar spacing of 12.5 cm.

Remark 19. Steel rebar oriented in the x_1 or x_2 directions of a same steel grid figures a different position in the thickness of the plate (i.e. along the x_3 direction), then inducing a significant variation in the bending stiffness of the plate around x_1 or x_2.

For all the simulations presented in this article, the unit cell mesh is composed of linear tetrahedral finite elements refined in the vicinity of steel rebar in order to represent as much as possible their cylindrical geometry. The average number of degrees of freedom considered is of 100,000.

An automated *python*™ process generates automatically the RVE mesh from the following eleven geometrical parameters:

1. Plate thickness H
2. and 3. Steel rebar spacing along x_1 and x_2
4. 5. 6. and 7. Diameters of the four steel rebar
8. 9. 10. and 11. x_3 positions of the four steel rebar

This three-dimensional mesh includes the splitting of nodes located on steel–concrete interfaces (surfaces Γ^ζ_b), the assignment of the different mesh zones to the sub-domains Ω^1_i, Ω^2_i, and periodicity of node locations for the external boundaries (normal unit vectors along x_1 and x_2). Microscopic material properties and boundary conditions prescribing, including periodicity in the RVE

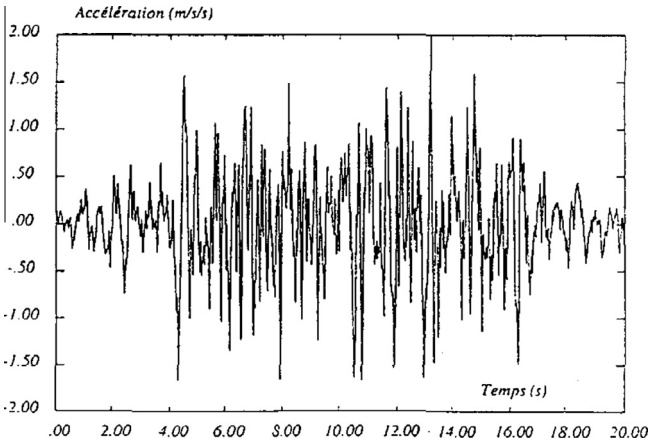

Fig. 5-2. Reference accelerogram for SAFE tests.

Table 5-2
Material properties for transverse and principal walls of SAFE experiments

E_A (GPa)	ν_A (–)	E_B (GPa)	ν_B (–)	α_+ (–)	α_- (–)	γ_+ (–)	γ_- (–)	σ_{d+} (MPa)	σ_{crit} (MPa)
200	0.3	24	0.2	1	3	−0.02	0.275	1.5	1.5

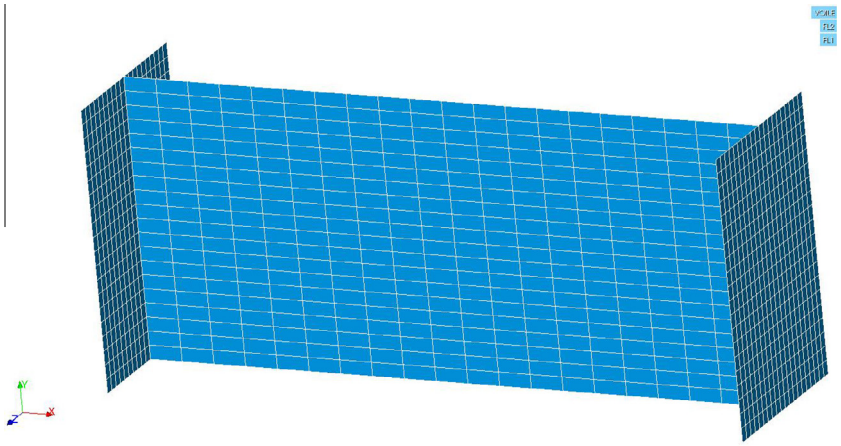

Fig. 5-3. Mesh for the simulation of SAFE experiments.

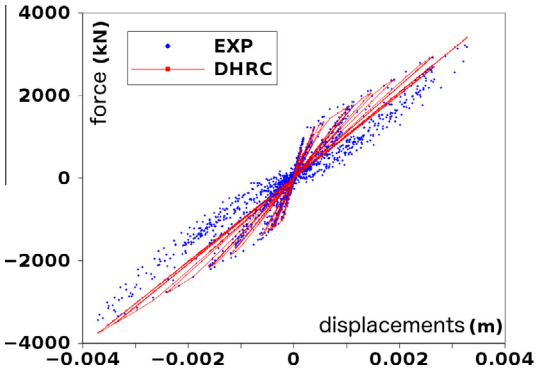

Fig. 5-4. Force–displacement responses for run 1 of SAFE experiments wall T5 – comparison between experiments (blue dots) and DHRC simulation (red line). (For interpretation of the references to color in this figure legend, the reader is referred to the web version of this article.)

outer surfaces (upper and lower surfaces remaining free) and bond slip basis function are set.

The results of the numerical finite element simulations are used to identify the 335 DHRC macroscopic parameters with the help of a standard least square algorithm.

4.2.5. Analytical trivial example

To illustrate the implementation of the previous approach, we take the following representative analytical trivial example.

The first step consists in verifying that the automatic procedure recovers the usual isotropic linear elastic plate stiffness tensor if we take, in the whole RVE, the same uniform sound elastic characteristics(E,ν). Indeed, in that case, the RVE Ω is reduced to the simple segment $]-\frac{H}{2},\frac{H}{2}[$ along the axis $(O\underline{e}_{x_3})$, and all the auxiliary fields $\underline{\chi}^{\alpha\beta}$ in membrane and $\underline{\xi}^{\alpha\beta}$ in bending depend only on x_3. Solving in such situation the auxiliary problems (3-4), using first trial $\underline{v}(x_3)$ functions $(v_1,v_2,0)$ then $(0,0,v_3)$, we obtain easily:

$$\underline{\chi}^{\alpha\alpha}=\frac{\nu}{1-\nu}(0,0,x_3);\quad \underline{\chi}^{12}=(0,0,0);\quad \underline{\xi}^{\alpha\alpha}=\frac{\nu}{2(1-\nu)}(0,0,x_3^2);\quad \underline{\xi}^{12}=(0,0,0) \tag{4-19}$$

hence the macroscopic homogenised elastic plate tensor $\mathbb{A}$:

$$\mathbb{A}^{mm}_{\alpha\alpha\alpha\alpha}=\frac{EH}{1-\nu^2};\ \mathbb{A}^{mm}_{\alpha\alpha\beta\beta}=\frac{\nu EH}{1-\nu^2};\ \mathbb{A}^{mm}_{1212}=\frac{EH}{2(1+\nu)};\mathbb{A}^{ff}_{\alpha\alpha\alpha\alpha}=\frac{EH^3}{12(1-\nu^2)};$$
$$\mathbb{A}^{ff}_{\alpha\alpha\beta\beta}=\frac{\nu EH^3}{12(1-\nu^2)};\ \mathbb{A}^{ff}_{1212}=\frac{EH^3}{24(1+\nu)};\ \mathbb{A}^{mf}=\mathbf{0} \tag{4-20}$$

5. Numerical results: reinforced concrete shear wall and building

5.1. SAFE experiments

One of the main loading conditions imposed to walls during earthquakes is in-plane distortion, or shear. Thus, the experimental benchmark SAFE of shear walls tested at CCR/ISPRA in 1998 (Favier et al., 1988) is chosen as first validation of the DHRC model.

5.1.1. General data

The benchmark SAFE gathers experimental data over thirteen shear walls of various dimensions. The wall T5 is the one of interest for this study since it is the closest to the type of wall used in nuclear power plants: it contains the highest steel proportion (0.8% of reinforcing ratio) and is the thickest (20 cm). This wall geometry is presented in Fig. 5-1. Several sets of seismic solicitations of increasing level were imposed successively to this wall and, in order to comply with the industrial context of interest, the series considered here corresponds to an equivalent run of 0.43 g.

As presented in Fig. 5-1, the considered wall is of length 2.6 m for a height of 1.2 m and a width of 20 cm. It is reinforced at both ends by two strengthening walls of same height and width and of a length of 80 cm. The wall is built with to rigid steel tie beams at its upper and lower ends that allow applying boundary conditions and loading, preventing any rotation of the specimen upper boundary.

As for the steel reinforcement, the wall contains 0.8% of steel rebar in each direction, which corresponds to a reinforcement constituted of two grids with square mesh of 125 mm, realised with steel rebar of diameter 10 mm and 12 mm alternatively. Horizontal rebar are disposed with a cover of 21 mm and vertical ones with a cover of 36 mm. As for the two strengthening walls, they contains horizontal rebar of diameter 12 mm with a spacing of 125 mm and cover of 15 mm and vertical ones gathered by pairs with diameter 14 mm, spaced of 125 mm and a cover of 28 mm.

Finally, the wall was submitted to five successive homothetic seismic loadings of increasing seismic level. The first run corresponds to a design seismic level and is the one that will be modeled in this paper. The used accelerogram is synthetic with an aimed design spectrum of 0.43 g (ZPA), and a standard pic frequency of 4 Hz. This accelerogram is plotted at Fig. 5-2.

Fracture tests in tension and compression on cubic and cylindrical test samples provided the following tension and compression strengths for concrete, sum up in Table 5-1. An average value of tests on cylindrical test samples is chosen. Young's modulus for

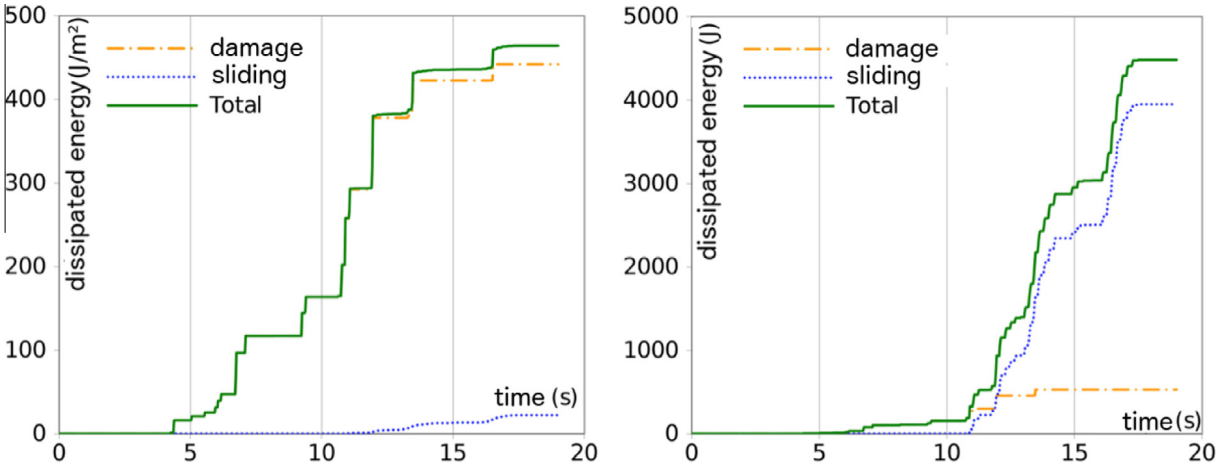

Fig. 5-5. Evolution of global (left) and nodal (right) dissipated energies over time.

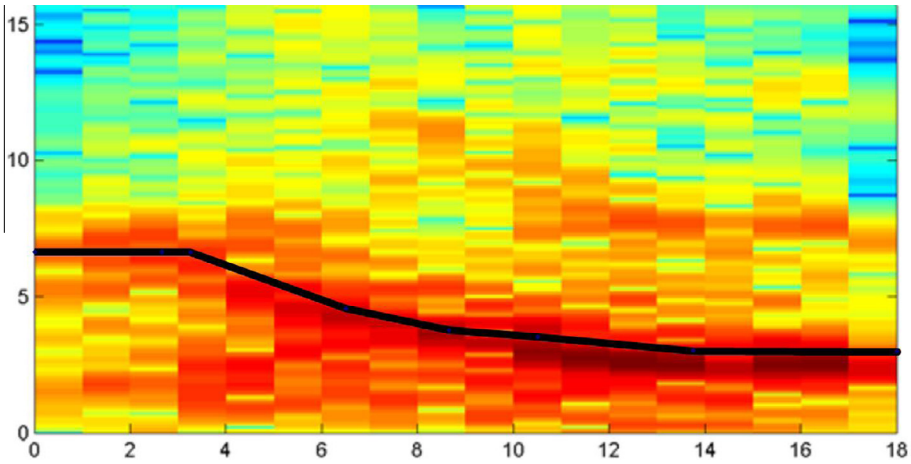

Fig. 5-6. Evolution of eigen-frequency of SAFE wall during solicitation. Comparison between experimental spectrogram (color map) and simulated eigen-frequency with numerical model DHRC (black line). (For interpretation of the references to color in this figure legend, the reader is referred to the web version of this article.)

concrete was not provided and will then be chosen according to design concrete codes: $E = 12000\, f_{c28}^{1/3}$. Tension tests on steel rebar gave us a Youn's modulus of 200 GPa.

5.1.2. Finite element model

The mesh used to represent this experiment is presented in Fig. 5-3. It is placed in the mean plane of the walls so that the length of the principal wall is 2.8 m on the mesh whereas it is 2.6 m in Fig. 5-1. The 2D elements used are DKT-DKQ thin plate finite element (Batoz, 1982). The finite element model is perfectly clamped to the ground.

5.1.3. DHRC parameters identification

Given that transverse walls and principal one present various geometrical properties, two different identification processes had to be computed. The material properties, however, are the same for both transverse and principal walls. The needed parameter values are sum up in Table 5-2 and result from experimental data. Since concrete Young's modulus was not provided, it has been chosen so that the simulated structural elastic stiffness corresponds to the experimental observed one.

5.1.4. Results

Fig. 5-4 compares the force–displacement response of the finite element model and the experiment. Here we can notice the degradation of global stiffness during the solicitation as well as a good prediction of the maximal force for each cycle and for the whole test. However, residual strains (sliding strains for our model) seem to be underestimated by the model.

One explication would be that the dissipative phenomenon inducing residual strains under distortion solicitation is not represented by our model, meaning that these solicitations do not activate internal steel/concrete sliding. As a confirmation, we can compare global dissipated energy over the whole principal wall and dissipated energy at a node located near a junction between principal and transverse wall (Fig. 5-5). We can then notice that sliding is the dominating phenomenon near transverse/principal walls junction but becomes of less importance when considering total dissipated energy density. Indeed, only a very few number of elements undergo sliding. These are the elements where some other solicitations than pure shear are in action (near junctions).

Finally, what interest most seismic engineers is the drop in peak-frequency of a system during seismic solicitation. By a post-treatment of the former simulation, we can compute, at the end of several time steps, the first peak-frequency of our structure, considering a density of 2.4 for concrete and 7.8 for steel and a

Fig. 5-7. Experimental SMART2008 mock-up. Left: bare specimen on shaking table; right: specimen on shaking table with additional masses during seismic test. © CEA/EMSI.

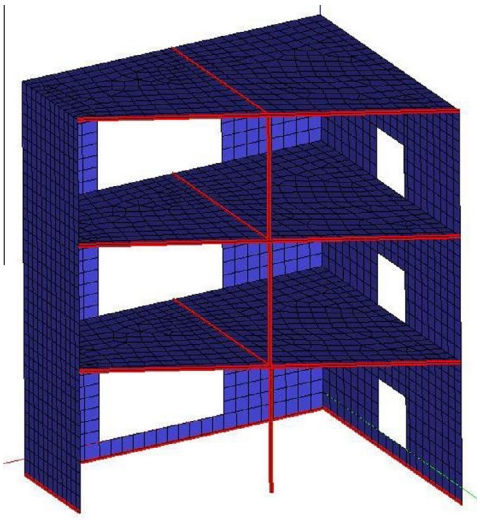

Fig. 5-8. Finite element mesh for numerical simulation of SMART2008 mock-up (red: beam elements, blue: DKT elements). (For interpretation of the references to color in this figure legend, the reader is referred to the web version of this article.)

total mass of 2818 t for the system on top of the mock-up. Experimental results are obtained from Fourier transform analysis on a sliding window over the whole length of the signal (Favier et al., 1988). This method produces a spectrogram representing frequency spectrum of the whole mock-up. Colours used here range from dark blue for low amplitudes to dark red for high ones (see Fig. 5-6).

A good correlation can be observed between experimental and numerical results, underlying the apparent good ability for DHRC model to represent the drop in eigen-frequency during seismic solicitation.

5.1.5. Discussion

SAFE experiments brought to light the inability of DHRC model to represent the phenomenon inducing residual displacement under distortion solicitation. However, DHRC model seems able to predict adequately the drop in global stiffness as well as the maximum force reached during solicitation. It is also efficient to represent the experimentally observed drop in eigen-frequency.

It is common to consider that distortion and shear are major solicitations when it comes to earthquakes. As a consequence, it could be interesting to try to validate our model on a realistic building in order to measure its adequacy when it comes to more complicated types of solicitations when we no longer have pure distortion.

5.2. SMART experiments

An experimental program named "SMART" ("Seismic design and best-estimate Methods Assessment for Reinforced concrete buildings subjected to Torsion and non-linear effects") was supported by Électricité de France (EDF) and Commissariat à l'Énergie Atomique et aux Energies Alternatives (CEA), and partially endorsed by the International Atomic Energy Agency (IAEA). Two reduced scale (1/4th) representative specimens of an asymmetric nuclear RC multi-storey building have been designed and tested on the AZALEE 6 degrees of freedom shaking table at CEA Saclay, the first one in 2008, the second one in 2012, the only noticeable difference lying in the foundation geometrical dimensions (Fontan et al., 2014). These experiments have the advantage to involve realistic RC slabs and walls and a large set of experimental measurements is available. Two international benchmarks have been organised using the experimental data from these seismic tests in particular in order to compare and validate the numerical models used to assess the dynamic response of RC structures under seismic loading (Smart2013_Organizing-team (2013)).

5.2.1. General data

The trapezoidal shaped mock-up made of RC has three floors (a RC beam –rectangular section 15 cm × 32.5 cm – and a RC column – square section 20 cm × 20 cm – give an additional stiffness to the building at each storey) and four walls with openings, supported on a continuous reinforced concrete footing (rectangular section 25 cm × 65 cm), see Fig. 5-7.

The overall dimensions are: 3.65 m high, 3.0 m × 2.5 m in plane. Its bare weight is about 11.89 t. Additional masses (total amount about 33.94 t) are located on the three floors to achieve the Cauchy–Froude's similitude law (acceleration, strain and stress conservation). It is anchored on the shaking table by means of a 0.02 m thick steel plate.

All the walls and floors are 10 cm thick. The steel reinforcement was designed according to the European design code EC2. The reinforcement grid in the wall consisted of primarily 4 mm diameter plain steel bars at 100 mm spacing which was supplemented by 8 mm or 6 mm diameter plain rebar near the wall openings and along the vertical direction in the whole first story walls.

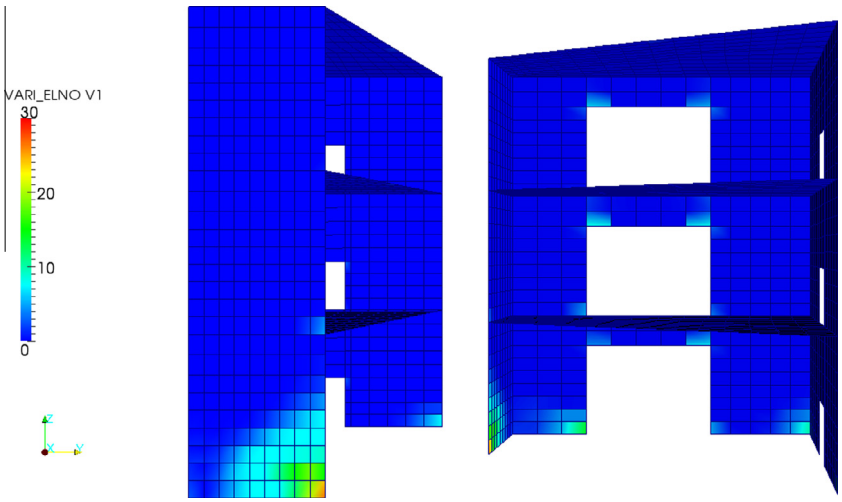

Fig. 5-9. Map of DHRC damage variable $\mathbf{D_1}$ at the end of simulation.

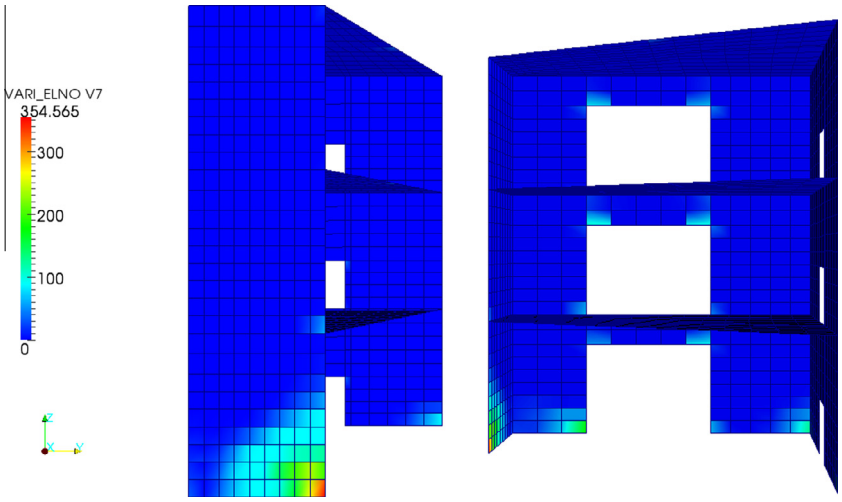

Fig. 5-10. Map of DHRC model sliding variable $\mathbf{E_2^{\eta 1}}$ at the end of simulation.

The mass centre and the effective torsion centre belong to different axes and thus the torsional effect resulting from the seismic loads is amplified and generates shear states inside the walls.

The seismic design of the mock-up was based on a 5% damped envelope design spectrum anchored at .2 g peak ground acceleration. A series of successive seismic loadings (pairs of accelerograms in the two horizontal directions) was applied to the mock-up ranging from low synthetic excitations to beyond design natural ground motions (up to 1.1 g peak ground acceleration).

We report hereafter in Table 5-3 the geometrical characteristics and mean material properties based on test concrete cylinders from actual casts of the SMART2008 as-built mock-up (strength at beginning of seismic tests) and steel bars tests. Concrete density is about 2300 kg/m^3 in the whole mock-up. Two symmetric rebar grids reinforce every wall and slab. Rebar cover is 10 mm (measured from ∅4 ties of transverse reinforcement).

From these material properties, we propose to choose the bond strength – not provided by benchmark organisers – according to the lower value proposed by CEB-FIP Model Code 1990 (1993) or Fernandes et al. (2013). Due to the choice of plain steel bars of ∅4 reinforcing grids remaining in the elastic domain, bond strength is then $1.8(\sigma_c')^{1/2}$, given in MPa, i.e. here about 11.3 MPa.

The position and spacing of every grid rebar in the thickness of the considered wall or slab is determined from reinforcement drawings provided by the benchmark organizers. These data are highly variable inside even one only wall, because reinforcement is often stronger near wall/slab intersections and at the places where strong tension is awaited (e.g. in the middle of a slab).

5.2.2. Finite element model

The SMART2008 mock-up is modelled by means of DKT thin plate finite element for the walls and floors and Timoshenko beam elements for the RC columns and beams. For the sake of simplicity, the SMART2008 finite element model is perfectly clamped onto the shaking table, considered as perfectly rigid, thus transferring the seismic signal as it to the mock-up. The RC columns and beams are considered to behave elastically. The number of DKT plate elements for the RC mock-up itself is 2576. The mesh is presented on Fig. 5-8.

Additional masses are idealised by a supplementary distributed surface density, in order to produce respectively for the 1st, 2nd, 3rd floors: 11.60, 12.0, 10.25 tons. The total weight is about 47 tons.

5.2.3. DHRC parameters identification

For the sake of simplicity, the mock-up is modelled with the same walls and slabs everywhere, with a uniform reinforcement. Thus, only one parameter identification is proceeded and its result

Table 5-3
SMART2008 mock-up geometrical and mean material properties.

Structural element	Section m × m thickness m	X rebar diameter mm	Y rebar diameter mm	Concrete E, ν elastic moduli GPa; –	Rebar E elastic modulus GPa	Concrete compressive strength σ_c' MPa	Concrete tensile strength MPa
Foundation	0.15 × 0.38	7∅8 inf; 7∅8 sup		25000; 0.17	190000	50.5	3.45
Wall 1st level	0.10	2 horiz. grids ∅4	2 vertical grids ∅6	30500; 0.19	267333	44.5	3.15
Slab 1st level and beam	0.15 × 0.325 0.10	2 grids ∅4;	2 grids ∅4;	29000; 0.17	267333	40.0	3.25
Wall 2nd level	0.10	2 horiz. grids ∅4	2 vertical grids ∅4	26700; 0.19	267333	37.5	2.70
Slab 2nd level and beam	0.15 × 0.325 0.10	2 grids ∅4;	2 grids ∅4;	31500; 0.17	267333	43.5	3.35
Wall 3rd level	0.10	2 horiz. grids ∅4	2 vertical grids ∅4	33500; 0.18	267333	40.0	4.00
Slab 3rd level and beam	0.15 × 0.325 0.10	2 grids ∅4;	2 grids ∅4;	29500; 0.18	267333	37.5	3.40
Column	0.20 × 0.20	8∅8 + 4∅10 on the first 40 cm from base		33500; 0.18	252666	40.0	3.25

Table 5-4
Experimental vs DHRC simulated results

	Initial eigen frequency (Hz)	Final eigen frequency (Hz)	Dissipated energy	
DHRC	9.07	8.26	120 J	damage 100 J
				sliding 20 J
Experiments	6.8	4.9	...	

is applied to the whole set of DKT elements in the mesh. The reference slab used to compute the parameter identification is the slab of level 1. One could notice that this approximation is not so strong given that the geometrical and mean material properties for the walls and slabs of the mock-up are roughly similar. The strongest approximation is the uniformity of reinforcement position and spacing. This could lead to a stronger degradation at the corners of the building – where slabs and walls meet – in the simulation than in reality where additional rebar are supposed to ensure the integrity of these elements.

5.2.4. Results

The mock-up was first subjected to low level seismic excitations (biaxial horizontal accelerograms obtained from the 5% damping design spectrum, corresponding to a Magnitude 5.5 earthquake at a distance of 10 km), by means of shaking table actuators, so that it would remain within the linear elastic range: this stage is designed in order to check all the modelling assumptions (geometry, boundary conditions, mass distribution, material data). Then, synthetic accelerograms ground motion sequence, scaled from the 1994 January 17th Northridge, California, earthquake main shock ($M_w = 6.7$, $PGA = 1.1g$ anchor level) PGA anchor level, are applied in both x, y directions. Our computations consider the regular sequence of scaled increasing ground motions, as during the experimental tests (Smart2013_Organizing-team (2013)).

The computation takes into account gravity, which constitutes a preliminary state of the model, before applying the seismic sequence.

The first results presented in Table 5-4 compare the experimental and simulated eigen-frequencies of the mock-up, using finite element software *Code_Aster* (Code Aster, 2001). It is clear that the simulated eigen-frequencies are way higher than the experimental peak-frequencies, which were determined by hammer shock tests. This difference can be explained by the simplistic assumption of a perfectly rigid shaking table in the FEM model, as pointed by the benchmark organizers (Smart2013_Organizing-team (2013)). However, the final eigen-frequency computed from the DHRC simulation – using the updated tangent stiffness matrix in the eigen-value problem solver – shows a drop of 9% related to the initial one, smaller than observed experimentally. This discrepancy about the drop of eigen-frequency – which is in accordance with the usual expectation that a damaged building will behave more smoothly than a sound one – is certainly attributable to the simplistic set of FEM modelling assumptions made before, in particular the boundary conditions. Moreover, the access to the two components of dissipated energy that are damage and sliding allow us to underline the importance of sliding in the energy dissipation of a RC building. Indeed, sliding dissipated energy contributes for one sixth in the total dissipated energy.

Figs. 5-9 and 5-10 present the state of damage variable D_1 (damage in the upper half of the plate) and sliding variable $E_2^{\eta 1}$ (sliding along horizontal bars in the upper half of the plate) at the end of the numerical simulation. The direct correlation between these two variables appears clearly as the damaged and sliding zones are the same. As expected we notice that dissipation is located at the corners of the structure and mostly near the perfect clamping onto the shaking table. This result correlates with experimental observations of surface cracking at these locations.

At this state, these qualitative results are only promising since we have to adopt more precise modelling assumptions to get numerical results closer to experimental values. However, the quantitative importance of sliding in total dissipated energy and the relatively short amount of time necessary to compute the whole simulation (about 8 h) are preliminary results emphasizing the importance of a proper homogenization process to build a model and identify its parameters and the computational and qualitative efficiency of such an *a priori* process.

5.2.5. Discussion

SMART benchmark allowed us to validate DHRC model on a realistic building. It seems that the model is good at representing qualitative experimental results and the importance of sliding appears to be more important on a complex building than on a simple shear wall. As a consequence, regarding the numerical results presented in this section, DHRC model can be considered as an efficient model to represent the homogenised behaviour of RC plates under seismic solicitations with damage and internal sliding at concrete/steel interface. Nevertheless, as the experimental conditions are rather complex, we will have to go beyond this

first numerical simulation to assess exhaustively the representativeness of the DHRC constitutive model.

6. Conclusion

By means of an averaging periodic homogenisation method within the framework of the Generalised Standard Material theory, we proposed a nonlinear stress resultant constitutive model for RC plate structural element global behaviour.

This nonlinear constitutive model accounts for damage resulting from diffuse micro-cracking of concrete and tangential debonding at steel bar – concrete interface, for cyclic loading paths. The homogenisation method secures the passage of both materials, concrete and steel bars, from the local scale to the overall one: (1) in determining the general formulation of the overall stress resultant constitutive model, in particular the macroscopic state functions including the membrane-bending coupling and energy dissipation, (2) in formulating an original coupling term between damage and steel–concrete debonding, inducing a better representation of energy dissipation during the material degradation, and (3) finally in defining the parameters identification procedure.

A certain number of assumptions have been proposed to make tractable the whole methodology, based on theoretical and experimental observations. These assumptions are not directly related to the particular choice of materials used in this study, so that the formulated constitutive model is actually more general and could be used in other types of applications.

The model parameters are identified from a restricted number of geometric and material characteristics of the considered RC structural element section. Using a direct implicit time integration method guaranteeing a robust algorithm, this homogenised constitutive model – called DHRC – has been implemented into the finite element software *Code_Aster*, allowing a wide range of practical applications in engineering. Convergence difficulties stemming from the softening behaviour of concrete are avoided thanks to steel rebar in the homogenisation of RC section. By comparing the obtained numerical results to experimental observations on an international benchmark, we assessed the ability of this homogenised constitutive model and its parameters identification procedure to predict the nonlinear cyclic behaviour of RC structures under seismic loading, in particular stiffness degradation and energy dissipation. However, it seems that other dissipative process in the RC section have to be taken into account to a better description of energy dissipation. This is the subject of a work in progress by Huguet et al. (2014), aiming at accounting for concrete stress transfer at cracks. Moreover, it could be interesting to deal with the modelling of rather short shear walls that are present in many RC buildings, to extend the DHRC constitutive plate model adding the transverse distortion modelling, within the Hencky–Mindlin plate theory framework. It could be useful to account for the contribution of transverse reinforcement in the RC section, including their role in the transverse shear behaviour. Indeed, this extension could be fairly easy, since it is possible to add the corresponding transverse distortion auxiliary problems in the homogenisation procedure, and then to deduce the supplementary terms in the free energy (Voldoire, 1993). Finally, another outlook would consist in the development of an appropriate derived boundary and connection constitutive homogenised model to complete this modelling tool, as it is known that any homogenised model are not entirely relevant near the boundaries of structures.

Acknowledgments

Authors wish to acknowledge Electricité de France, R and D Division, Université Pierre et Marie Curie and Association Nationale de la Recherche et de la Technologie for their financial and material support for conducting these researches. This research reported in this paper has been supported in part by the SEISM Institute (http://www.institut-seism.fr). Fruitful discussions with Professor Jean-Jacques Marigo at École Polytechnique and Eric Lorentz of Électricité de France, as well as contributions by Sébastien Fayolle and Medhi Tha in the numerical calculations and implementation updating in *Code_Aster*, are also gratefully acknowledged. Authors are particularly indebted to Dr. Sébastien Fayolle for very useful comments and checking on the numerical implementation. Finally, they will thank the anonymous reviewers' comments in improving the manuscript.

Appendix A. Proof of the zero-valued tensor $\boldsymbol{B}$ if microscopic damage field is symmetric with respect to central planes in the RVE

Let us recall that the tensor $\mathbb{B}$ components are defined by: $\mathbb{B}^{m\zeta}_{\alpha\beta\gamma}(\boldsymbol{D}) = \langle\langle \mathbb{a}_{\alpha\beta kl}(d) : \varepsilon_{kl}(\underline{\chi}^{\eta_{\gamma\zeta}})\rangle\rangle_\Omega$ and $\mathbb{B}^{f\zeta}_{\alpha\beta\gamma}(\boldsymbol{D}) = -\langle\langle x_3 \cdot \mathbb{a}_{\alpha\beta kl}(d) : \varepsilon_{kl}(\underline{\chi}^{\eta_{\gamma\zeta}})\rangle\rangle_\Omega$, see (3-13) and (3-14). Let us assume that the components of the concrete damaged elastic tensor are symmetric with respect to the plane $x_1 = 0$, i.e. Γ_s ; moreover, according to Section 3.2, this tensor fulfils the symmetries with respect to the reference frame. Let us consider the auxiliary problem (3-6) concerning the corrector $\underline{\chi}^{\eta^\rho_1}$ associated to sliding in the x_1 direction. Necessarily, we have the following properties: $\chi_1^{\eta^\rho_1}$ is symmetric with respect to the plane $x_1 = 0$, whereas $\chi_2^{\eta^\rho_1}$ and $\chi_3^{\eta^\rho_1}$ are antisymmetric. Therefore, $\mathbb{a}_{iikl}(d) : \varepsilon_{kl}\left(\underline{\chi}^{\eta^\zeta_1}\right)$ and $\mathbb{a}_{23kl}(d) : \varepsilon_{kl}\left(\underline{\chi}^{\eta^\zeta_1}\right)$ are antisymmetric with respect to the plane $x_1 = 0$, whereas $\mathbb{a}_{1jkl}(d) : \varepsilon_{kl}\left(\underline{\chi}^{\eta^\zeta_1}\right)$ are symmetric, for $j \neq 1$ and $\mathrm{a}_{1jkl}(d) : \varepsilon_{kl}\left(\underline{\chi}^{\eta^\zeta_1}\right)$ are antisymmetric with respect to the plane $x_2 = 0$.

Performing the integration on the whole RVE, we deduce that: $\mathbb{B}^{m\zeta}_{\beta\delta\lambda}(\boldsymbol{D})$ and $\mathbb{B}^{f\zeta}_{\beta\delta\lambda}(\boldsymbol{D})$ vanish. The same reasoning holds for the other direction in the mid-plane of the RVE.

Since the tensor $\mathbb{B}$ manages the coupling between RC plate kinematics and steel bond sliding, we conclude that bond sliding can occur only if symmetry loss appears in the RVE, due to damage.

References

Andrieux, S., Bamberger, Y., Marigo, J.-J., 1986. Un modèle de matériau microfissuré pour les roches et les bétons. J. Méca. Théo. Appl. 5, 471–513.

Anyfantis, K.-N., 2014. On the failure analysis of bondlines: stress or energy fracture criteria? Eng. Fract. Mech. 126, 108–125.

Asprone, D., Frascadore, R., Di Ludovico, M., Prota, A., Manfredi, G., 2012. Influence of strain rate on the seismic response of RC structures. Eng. Struct. 35, 29–36.

Batoz, J.-L., 1982. An explicit formulation for an efficient triangular plate-bending element. Int. J. Numer. Methods Eng. 18, 1077–1089.

Bazant, Z.-P., Oh, B.-H., 1983. Crack band theory for fracture of concrete. Mater. Struct. 16 (93), 155–177.

Benmansour, M.-B., 1997. Modélisation du comportement cyclique alterné du béton armé. Application à divers essais statiques de poteaux. Paris, France (PhD thesis). École Nationale des Ponts et Chaussées.

Caillerie, D., Nedelec, J.-C., 1984. Thin elastic and periodic plates. Math. Methods Appl. Sci. 6, 159–191.

CEB-FIP Model Code 1990, 1993. Bulletin d'information No. 195–196: Comité Euro-International du Béton, Fédération Internationale de la Précontrainte.

Chaboche, J.-L., 2003. Damage mechanics. In: Milne, I., Ritchie, R., Karihaloo, B. (Eds.), Comprehensive Structural Integrity, vol. 2. Elsevier Ltd, Oxford, pp. 213–284.

Ciarlet, P.-G., 1979. A justification of a nonlinear model in plate theory. Comput. Methods Appl. Mech. Eng. 17–18 (Part 1), 227–254.

Code Aster, 2001. General public licensed structural mechanics finite element software. From <http://www.code-aster.org>.

Combescure, C., Dumontet, H., Voldoire, F., 2013. Homogenised constitutive model coupling damage and debonding for reinforced concrete structures under cyclic solicitations. Int. J. Solids Struct. 50 (24), 3861–3874.

Destuynder, P., Theodory, C., 1986. Homogénéisation de structures minces en béton armé. RAIRO-Modélisation mathématique et analyse numérique, 20, n°1, 47–74.
Einav, I., Houlsby, G.-T., Nguyen, G.-D., 2007. Coupled damage and plasticity models derived from energy and dissipation potentials. Int. J. Solids Struct. 44, 2487–2508.
Eligehausen, R., Popov, E., Bertero, V., 1983. Local Bond Stress-Slip Relationships of Deformed Bars Under Generalized Excitations: Experimental Results and Analytical Model. Earthquake Engineering Research Center, College of Engineering, University of California.
Favier, D., Guelin, P., Tourabi, A., Wack, B., Pegon, P., 1988. Ecrouissages-Schémas thermomécaniques et a variables internes: méthode de définition utilisant le concept d'hystérésis pure. Arch. Mech. 40 (5–6), 611–640.
Feenstra, P., De Borst, R., 1996. A composite plasticity model for concrete. Int. J. Solids Struct. 33 (5), 707–730.
Fernandes, C., Varum, H., Costa, A., 2013. Importance of the bond–slip mechanism in the numerical simulation of the cyclic response of RC elements with plain reinforcing bars. Eng. Struct. 56, 396–406.
Feyel, F., 1999. Multiscale FE2 elastoviscoplastic analysis of composite structures. Comput. Mater. Sci. 16, 344–354.
Fontan, M., Richard, B., Mazars, J., Capra, B., Cherubini, S., 2014. Benchmark SMART2013: from experiment to the numerical modeling. TINCE 2014. Paris (France).
Halphen, B., Nguyen, Q.-S., 1975. Sur les matériaux standards généralisés. J. de Mécanique 14, 39–63.
Hill, R., 1972. On constitutive macro-variables for heterogeneous solids at finite strain. Proc. R. Soc. London Ser. A 326, 131–147.
Huguet, M., Voldoire, F., Kotronis, P., Erlicher, S., 2014. Homogenized global nonlinear constitutive model for RC panels under cyclic loadings. In: 11th World Congress on Computational Mechanics (WCCM XI). Barcelona.
Kachanov, L.-M., 1958. Time of the rupture process under creep conditions. IVZ Akad. Nauk, S.S.R Otd. Tech. Nauk. 8, 26–31.
Krätzig, W.-B., Pölling, R., 2004. An elasto-plastic damage model for reinforced concrete. Comput. Struct. 82, 1201–1215.
Li, B., Maekawa, K., Okamura, H., 1989. Contact density model for stress transfer across cracks in concrete. J. Faculty Eng. Univ. Tokyo 40, 9–52.
Marti, P., Alvarez, M., Kaufmann, W., Sigrist, V., 1998. Tension chord model for structural concrete. Struct. Eng. Int. 8, 287–298.
Melo, J., Fernandes, C., Varum, H., Rodrigues, H., Costa, A., Arêde, A., 2011. Numerical modelling of the cyclic behaviour of RC elements built with plain reinforcing bars. Eng. Struct. 33 (2), 273–286.
Michel, J.C., 1984. Homogénéisation de matériaux élastoplastiques avec cavités (Doctoral dissertation).
Murcia-Delso, J., Stavridis, A., Shing, B., 2011. Modeling the bond-slip behaviour of confined large-diameter reinforcing bars. In: COMPDYN 2011, III ECCOMAS Thematic Conference on Computational Methods in Structural Dynamics and Earthquake Engineering. Corfu, Greece.
Nedjar, B., 2001. Elastoplastic-damage modeling including the gradient of damage formulation and computational aspects. Int. J. Solids Struct. 38, 5421–5451.
Nguyen, Q.-S., 1977. On the elastic plastic initial-boundary value problem and its numerical integration. Int. J. Numer. Methods Eng. 11, 817–832.
Pensée, V., Kondo, D., 2001. Une analyse micromécanique 3-D de l'endommagement par mésofissuration. C.R. Acad. Sci., Ser. IIb: Mec. 329, 271–276.
Pimentel, M., Brüwhiler, E., Figueiras, J., 2010. Extended cracked membrane model for the analysis of RC panels. Eng. Struct. 32, 1964–1975.
Richard, B., Ragueneau, F., 2013. Continuum damage mechanics based model for quasi brittle materials subjected to cyclic loadings: formulation, numerical implementation and applications. Eng. Fract. Mech., 383–406
Sanchez-Palencia, E., 1980. Non-homogeneous Media and Vibration Theory. Lecture Notes in Physics, vol. 127. Springer, Berlin.
Sanchez-Palencia, E., Zaoui, A., Suquet, P., 1987. Homogenization Technique for Composite Media. Springer, Berlin, Heidelberg.
Shao, J.-F., Jia, Y., Kondo, D., Chiarelli, A.-S., 2006. A coupled elastoplastic damage model for semi-brittle materials and extension to unsaturated conditions. Mech. Mater. 38, 218–232.
Simo, J.-C., Taylor, R.-L., 1985. Consistent tangent operators for rate-independent elastoplasticity. Comput. Methods Appl. Mech. Eng. 48, 101–118.
Smart2013_Organizing-team, 2013. SMART 2013 Benchmark. From <http://smart2013.eu/>.
Stolz, C., 2010. Thermodynamical description of running discontinuities: Application to friction and wear. Entropy 12 (6), 1418–1439.
Suquet, P., 1987. Elements of homogenization for inelastic solid mechanics. In: Sanchez-Palencia, E., Zaoui, A. (Eds.), Homogenization Techniques for Composite Media, Lecture Notes in Physics, vol. 272. Springer-Verlag, Berlin, pp. 193–278.
Suquet, P., 1993. Overall potentials and extremal surfaces of power law or ideally plastic composites. J. Mech. Phys. Solids 41, 981–1002.
Voldoire, F. (1993). Homogénéisation des structures hétérogènes. ISSN 1161-0611. Collection de notes internes de la Direction des Etudes et Recherches. Électricité de France.
Yvonnet, J., Gonzalez, D., He, Q.-C., 2009. Numerically explicit potentials for the homogenization of nonlinear elastic heterogeneous materials. Comput. Methods Appl. Mech. Eng. 198, 2723–2737.